

1 **Sediments in sea ice drive the Canada Basin surface**
2 **Mn maximum: insights from an Arctic Mn ocean**
3 **model**

4 **B. Rogalla¹, S. E. Allen¹, M. Colombo¹, P. G. Myers², K. J. Orians¹**

5 ¹Department of Earth, Ocean, and Atmospheric Sciences, University of British Columbia, Vancouver,
6 British Columbia V6T1Z4, Canada

7 ²Department of Earth and Atmospheric Sciences, University of Alberta, 1-26 ESB, Edmonton, Alberta
8 T6G2E3, Canada

9 **Key Points:**

- 10 • We present an ocean model of Mn in the Canadian Arctic that captures observed
11 spatial variation
- 12 • Non-local sediments transported by sea ice are a key source of micronutrients such
13 as Mn to the Canada Basin
- 14 • Rivers are most important for Mn in coastal regions of the Canadian Arctic

Corresponding author: Birgit Rogalla, brogalla@eoas.ubc.ca

Abstract

Biogeochemical cycles in the Arctic Ocean are sensitive to the transport of materials from continental shelves into central basins by sea ice. However, it is difficult to assess the net effect of this supply mechanism due to the spatial heterogeneity of sea ice content. Manganese (Mn) is a micronutrient and tracer which integrates source fluctuations in space and time. The Arctic Ocean surface Mn maximum is attributed to freshwater, but studies struggle to distinguish sea ice and river contributions. Informed by observations from 2009 IPY and 2015 Canadian GEOTRACES cruises, we developed a three-dimensional dissolved Mn model within a 1/12 degree coupled ocean-ice model centered on the Canada Basin and the Canadian Arctic Archipelago (CAA). Simulations from 2002-2019 indicate that annually, 87-93% of Mn contributed to the Canada Basin upper ocean is released by sea ice, while rivers, although locally significant, contribute only 2.2-8.5%. Downstream, sea ice provides 34% of Mn transported from Parry Channel into Baffin Bay. While rivers are often considered the main source of Mn, our findings suggest that in the Canada Basin they are less important than sea ice. However, within the shelf-dominated CAA, both rivers and sediment resuspension are important. Climate induced disruption of the transpolar drift may reduce the Canada Basin Mn maximum and supply downstream. Other micronutrients found in sediments, such as Fe, may be similarly affected. These results highlight the vulnerability of the biogeochemical supply mechanisms in the Arctic Ocean and the subpolar seas to climatic changes.

Plain Language Summary

Autumn storms on the Siberian side of the Arctic Ocean churn up sediment that freezes into sea ice. The prevailing ocean currents and winds push this sea ice across the Arctic Ocean towards the Canada Basin, where it melts and releases the sediment into the ocean. Sediment contains manganese and other nutrient elements that help support plankton and life. Using our manganese ocean model, 87-93% of Mn in the Canada Basin comes from “dirty” sea ice from 2002 to 2019, while rivers supply 2.2-8.5%. As a result of climate change, less dirty sea ice may make it across the Arctic Ocean, which could reduce this supply system of manganese and other similar micronutrients. This change also has potential impacts downstream: water from the Canada Basin travels through the shallow Canadian Arctic Archipelago into Baffin Bay and eventually the North Atlantic. We found that about 34% of Mn transported along this route comes from “dirty”

47 sea ice. In the Canadian Arctic Archipelago, other sources contribute as well: tides churn
48 up sediments from the ocean floor and many rivers flow into the channels. Our study
49 highlights ways in which climate change may impact the nutrient supply systems in the
50 Arctic Ocean.

51 **1 Introduction**

52 As the sea ice regime in the Arctic Ocean transitions from multi-year ice to pre-
53 dominantly first-year ice with overall reductions in sea ice extent, thickness and altered
54 drift patterns (Stroeve et al., 2012; Stroeve & Notz, 2018; Spreen et al., 2011; Kwok et
55 al., 2013), biogeochemical cycles and primary productivity are impacted through changes
56 to the sea ice supply mechanism. The Arctic Ocean continental shelves connect land and
57 ocean through the transfer of river runoff and sea ice from near-shore regions to the cen-
58 tral basins (Charette et al., 2016). Reductions in sea ice export from the shelves weak-
59 ens the long range transport of ice-rafted matter (Krumpen et al., 2019), including sed-
60 iments (Dethleff et al., 2000; Darby et al., 2011), nutrients and trace metals (Tovar-Sánchez
61 et al., 2010; Measures, 1999), pollutants (Pfirman et al., 1995; Peeken et al., 2018) and
62 climate-relevant gases (Damm et al., 2018), to the surface ocean in regions far away from
63 boundary sources. It is challenging to quantify the contribution of materials supplied by
64 sea ice with observations alone due to the high spatial and temporal variability in the
65 amount of sediment in sea ice and because it is difficult to distinguish it from additional
66 contributions to the surface ocean such as river runoff. However, it is clear that changes
67 to the physical processes in the Arctic Ocean will have impacts on the biogeochemical
68 cycles and primary productivity of the basins themselves, as well as downstream in sub-
69 polar seas (Drinkwater & Harding, 2001; Greene & Pershing, 2007).

70 Continental shelves cover half of the area of the Arctic Ocean (Jakobsson, 2002)
71 and their shallow depths facilitate the incorporation of suspended matter into sea ice as
72 it forms (Kempema et al., 1989). The narrow and deeper North American shelves are
73 not as important for basin-wide sea ice sediment transport as the wide Siberian shelves
74 (Eicken et al., 2005). In the Siberian shelf regions, fast ice builds up near shore in the
75 fall, coinciding with storm-related resuspension events, forming sediment-rich sea ice (Nürn-
76 berg et al., 1994). The transpolar drift transports this sea ice, as well as some ice from
77 the Chukchi Sea, towards the North Pole and the anticyclonic Beaufort Gyre redirects
78 a portion into the Canada Basin (T. Martin & Gerdes, 2007). This passage takes sev-

79 eral years, during which the ice undergoes cycles of melting, freezing and deformation.
80 The materials released by melt alter the geochemical signature of the underlying water
81 (Pfirman et al., 1995). Several studies indicate an increase in sea ice exchange caused
82 by faster ice drift speeds (Spreen et al., 2011; Kwok et al., 2013; Newton et al., 2017; Kipp
83 et al., 2018); however a recent study indicates a disruption in long range sea ice trans-
84 port due to the melt of first-year ice before it is incorporated into the transpolar drift
85 (Krumpfen et al., 2019). Reductions in long range sea ice transport can impact the sup-
86 ply of freshwater and nutrients to the surface ocean at the end of the transpolar drift
87 namely: Fram Strait, and indirectly the Canada Basin, the Canadian Arctic Archipelago
88 (CAA), and the subpolar North Atlantic. In order to establish the importance of sed-
89 iment from sea ice for biogeochemical cycles in the indirectly impacted regions of the Canada
90 Basin and the Canadian Arctic Archipelago, we developed a model of dissolved manganese
91 (Mn).

92 Mn is a reactive trace element and an important micronutrient which shares many
93 sources with iron (Fe) in the Arctic Ocean (Brand et al., 1983; Bruland et al., 1991; Jensen
94 et al., 2020). Mn has a scavenged-type profile with high concentrations near sources and
95 low background concentrations. This contrast makes it a convenient source tracer. Over
96 the Arctic Ocean shelves, sediment resuspension contributes Mn to the lower water col-
97 umn (Evans & Nishioka, 2018; Colombo et al., 2020). Pacific water from the Bering Strait
98 and Chukchi Sea is a source of Mn to the halocline of the Arctic Ocean (Jensen et al.,
99 2020; Colombo et al., 2020). Mn is typically highest at the surface where atmospheric
100 deposition, river runoff and ice melt contribute, and where photo-reduction of Mn is en-
101 hanced and bacterially-mediated Mn oxidation is inhibited (Sunda & Huntsman, 1994).
102 In the Arctic Ocean, this surface maximum is attributed to freshwater sources (Campbell
103 & Yeats, 1982; Yeats & Westerlund, 1991; Middag et al., 2011b; Cid et al., 2012; Kondo
104 et al., 2016; Colombo et al., 2020). Observational studies have identified the origin of
105 this freshwater as river discharge (Campbell & Yeats, 1982; Yeats & Westerlund, 1991;
106 Evans & Nishioka, 2018), sea ice meltwater (Measures, 1999; S. Wang et al., 2014, for
107 Fe), or a combination of both (Middag et al., 2011b; Cid et al., 2012; Kondo et al., 2016;
108 Colombo et al., 2020). Mn concentrations in rivers are significantly higher than in the
109 ocean (Colombo et al., 2019). Similarly, trace metals and nutrients in sea ice occur in
110 concentrations in excess of those in the ocean (Campbell & Yeats, 1982; Hölemann et
111 al., 1999; Granskog et al., 2003; Krachler et al., 2005; Aguilar-Islas et al., 2008; Tovar-

112 Sánchez et al., 2010; Kondo et al., 2016; Evans & Nishioka, 2018). The relative impor-
113 tance of river runoff and sea ice depends in part on the distance from the source and the
114 modification of input to the ocean (Fichot et al., 2013). The Canada Basin is distant from
115 land sources, while the narrow and shallow systems of channels that make up the CAA
116 are in close contact with the land-ocean interface and are more directly impacted by bound-
117 ary processes such as river discharge and sedimentary inputs (Colombo et al., 2021). We
118 will investigate the hypothesis that sediments transported by sea ice are an important
119 source of Mn in the Canada Basin, as suggested for reactive trace metals by Measures
120 (1999).

121 In order to distinguish the individual importance of external Mn sources within the
122 Canada Basin and the CAA, model studies are needed. Past studies have used tracers
123 such as terrestrial dissolved organic matter to trace river runoff on the scale of months
124 to years (Fichot et al., 2013; Mann et al., 2016) and the oxygen isotope ratio (Yamamoto-
125 Kawai et al., 2009) to distinguish the meteoric and sea ice melt contributions to fresh-
126 water in the Canada Basin. Mn is an interesting complementary tracer: it can trace both
127 the impact of river runoff and sediments in sea ice, and incorporates information about
128 chemical transformation such as redox conditions and removal over time, thereby help-
129 ing inform freshwater influence on biogeochemical cycling. Mn is also an essential mi-
130 cronutrient and integrates processes that fluctuate on short time scales. As a result, Mn
131 helps address one of the main limitations of the study of sediment entrainment and ex-
132 port events by sea ice: that they are episodic and localized in nature (Eicken et al., 2005).
133 Similarly, while sediment resuspension occurs intermittently, Mn integrates the effect of
134 this component on the lower water column. After establishing the contributions of the
135 Mn sources, we use Mn as a tool to study the general role of sea ice transport for bio-
136 geochemical cycles.

137 In this paper, we present a model of Mn in the Canadian Arctic Archipelago and
138 the Canada Basin, informed by in situ observations collected during the 2009 IPY GEO-
139 TRACES cruise (Sim, 2018) and the 2015 Canadian GEOTRACES cruises (Colombo
140 et al., 2020). Our work builds on the comprehensive first global model of Mn in the ocean
141 (Van Hulst et al., 2017) and previous smaller scale models of Mn in the North Pacific
142 Ocean (Johnson et al., 1996) and near hydrothermal vents (Lavelle et al., 1992). We in-
143 corporate new parameterizations for sediment resuspension, release of shelf sediments
144 in sea ice, and fluvial contributions, to capture the drivers of Mn distributions in the Cana-

145 dian Arctic. With this model, we show that the long range transport of sediments by
146 sea ice from the Siberian shelves drives the surface Mn maximum in the Canada Basin
147 while rivers are important in coastal regions. Using these results, we discuss implications
148 of future sea ice melt on Mn and Fe nutrient budgets in the Canada Basin and down-
149 stream in the Canadian Arctic Archipelago and Baffin Bay.

150 **2 Methods**

151 **2.1 Coupled Ocean-Ice Model**

152 For our simulations, we use ocean and ice dynamics calculated by the Arctic and
153 Northern Hemispheric Atlantic (ANHA12) configuration (Hu et al., 2018) of the Nucleus
154 for European Modelling of the Ocean (NEMO) version 3.4 (Madec, 2008). The ANHA12
155 configuration has a nominal horizontal resolution of $1/12^\circ$ which resolves freshwater fluxes
156 associated with coastal currents in the CAA, as well as eddies (Bacon et al., 2014; Chel-
157 ton et al., 1998). The position of the grid’s artificial pole in Northern Canada increases
158 the resolution in the CAA to about 2-3 km (Fig. 1). In the vertical, there are 50 depth
159 levels ranging from 1 m thickness at the surface to 454 m near the bottom. The bottom
160 bathymetry is represented using partial steps.

161 The ANHA12 domain has two open boundaries: one in Bering Strait and the other
162 at 20°S in the Atlantic Ocean. These boundaries are forced with Global Ocean Reanal-
163 yses and Simulations data (Masina et al., 2017). The ocean surface is forced with hourly
164 atmospheric data from the Canadian Meteorological Centre’s global deterministic pre-
165 diction system (Smith et al., 2014) and the rivers are forced with monthly runoff clima-
166 tology with enhanced Greenland melt runoff (Dai et al., 2009; Bamber et al., 2012). The
167 river forcing from 2010 is repeated for the following years (Hu et al., 2019).

168 The sea ice in ANHA12 is represented using the dynamic and thermodynamic Louvain-
169 la-Neuve (LIM2) sea ice model with an elastic-viscous-plastic ice rheology (Fichefet &
170 Maqueda, 1997; Bouillon et al., 2009). An evaluation of LIM2 in the ANHA12 config-
171 uration is provided by Hu et al. (2018). The general spatial distribution of ice thickness
172 within the Canada Basin and the CAA is captured well. However, sea ice concentration
173 and thickness are overestimated in the Canada Basin, likely because of underestimated
174 melt (Grivault et al., 2018; Hu et al., 2019). In the northern CAA, the model has very
175 thick sea ice (> 4 m), the central CAA has intermediate thickness ice (2.5-3 m), and there

176 is thin (< 2 m) ice in the eastern and southern channels of the CAA. The ANHA12 sim-
177 ulations are limited by the lack of a land-fast ice parameterization, resulting in ice ve-
178 locities that are higher than observed in Parry Channel, impacting the winter transport
179 (Grivault et al., 2018). In addition, tides are not included and as a result, the polynyas
180 which form due to tidally enhanced mixing are not well reproduced (Hughes et al., 2018).

181 The advection and diffusion of tracers are calculated within NEMO by the TOP
182 engine (Gent et al., 1995; Lévy et al., 2001). Tracer advection is calculated with the To-
183 tal Variance Dissipation (TVD) scheme (Zalesak, 1979) and we use the Flow Relaxation
184 Scheme (FRS) for the tracer boundary conditions. The vertical diffusion of tracers is cal-
185 culated from the Turbulent Kinetic Energy closure scheme within ANHA12 and the hor-
186 izontal eddy diffusivity parameter is set to $50.0 \text{ m}^2 \text{ s}^{-1}$.

187 **2.2 Model of Mn in the Canadian Arctic**

188 The Mn model runs offline in NEMO version 3.6 using five day averaged dynam-
189 ics fields from the ANHA12 reference run from January 2002 to December 2019 (Hu et
190 al., 2018). The Mn model consists of two main sets of computations: the advection and
191 diffusion of tracers calculated by the NEMO-TOP engine (Gent et al., 1995; Lévy et al.,
192 2001), and the source and sink contributions. The source and sink parameterizations were
193 developed guided by observations from the 2015 Canadian GEOTRACES cruises (Colombo
194 et al., 2020) and inspired by the first global model of Mn (Van Hulst et al., 2017). In
195 order to reduce the computational cost, we calculate the model on a sub-domain of ANHA12,
196 centered on the CAA (Fig. 1). Note that since we run offline, the physics originates from
197 the full domain.

198 The known sources and sinks of Mn in the ocean are: rivers, hydrothermal vents,
199 sediment diffusion, sediment resuspension, reversible scavenging, sinking, uptake and rem-
200 ineralization, atmospheric dust deposition, and flux from ice (Middag et al., 2011b; Balzer,
201 1982; Klinkhammer & Bender, 1980; Evans & Nishioka, 2018). From this list, we incor-
202 porate the processes that are important for dissolved Mn in the Arctic (summarized in
203 Fig. 2 and Eqn. 1 and 2). We directly model dissolved Mn(II), dMn, and oxidised Mn(IV),
204 oMn, for reversible scavenging (similar to Van Hulst et al., 2017, Eqn. 2). We do not
205 directly trace lithogenic particles containing Mn, i.e. particle-bound Mn (pMn), but we
206 incorporate their indirect effect through dissolution. We did not incorporate hydrother-

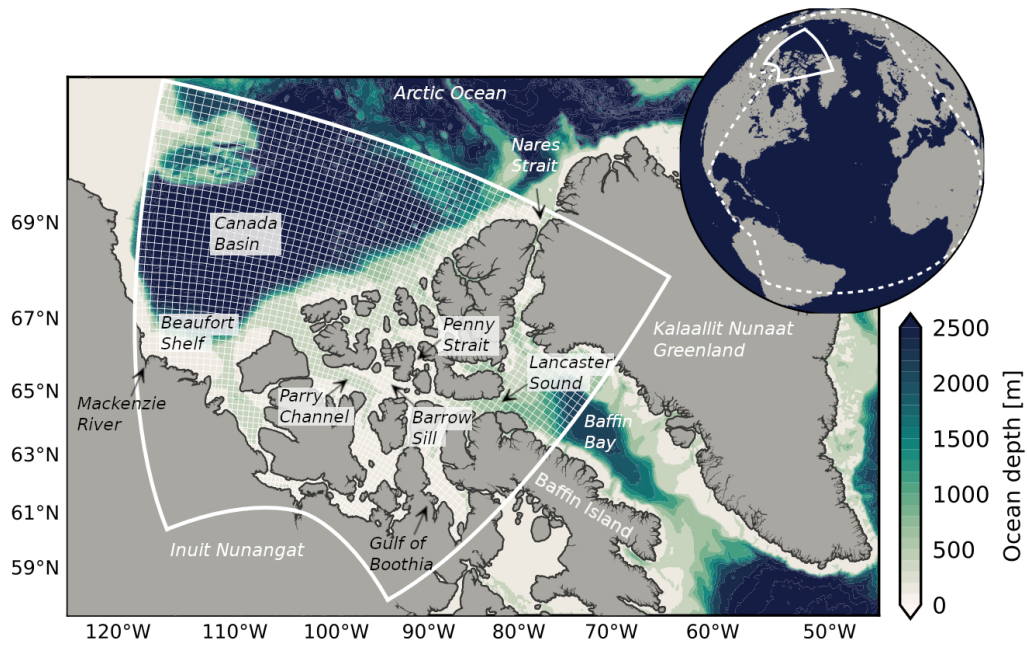


Figure 1. The Mn model domain is centered on the Canadian Arctic Archipelago with highest horizontal resolution in the south (about 3 km). The nominal horizontal resolution of the grid is $1/12^\circ$; the thin white grid depicts one in every ten ocean grid points. The solid white line shows the Mn model domain extent, while the dashed white line in the inset globe delineates the domain of the Arctic and Northern Hemispheric Atlantic configuration (Hu et al., 2018) of the ocean-ice model.

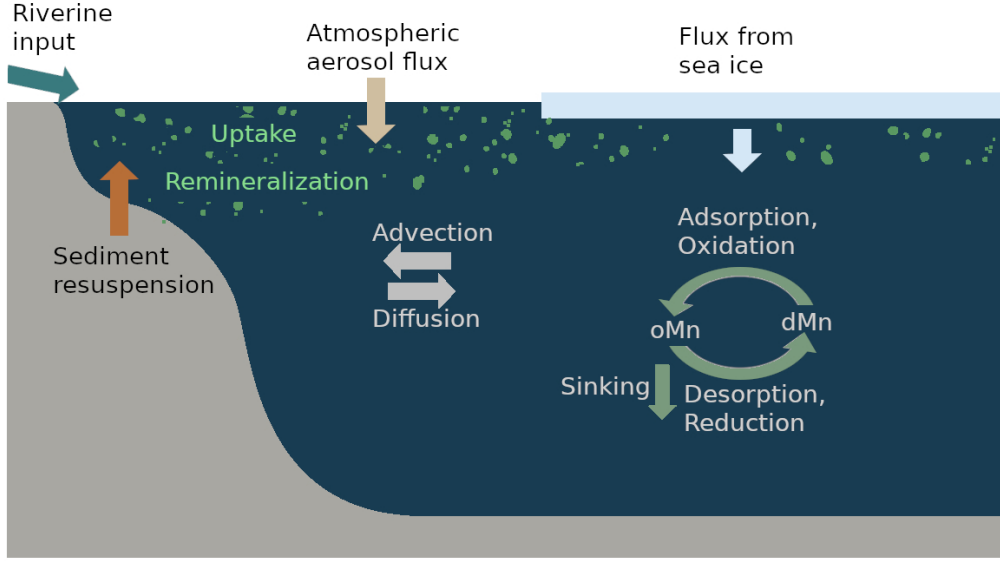


Figure 2. Summary of the processes that affect dissolved Mn (dMn) and oxidised Mn (oMn) concentrations in the Canadian Arctic Archipelago and the Canada Basin.

207 mal vents as a source of Mn in the Arctic, since the influence of the Gakkel Ridge is re-
 208 stricted to Nansen and Amundsen Basins due to scavenging nearby the source (Lavelle
 209 et al., 1992; Middag et al., 2011b). We also do not include sediment diffusion (reductive
 210 dissolution) because observations have indicated that these processes are not significant
 211 for Mn in the CAA (Colombo et al., 2020). The Mn model equations are:

$$\frac{\partial dMn}{\partial t} = S_{river} + S_{sediment} + S_{atm} + S_{ice} + S_{sed\ ice} + S_{bio} + R_{scav} + \text{advection} + \text{diffusion} \quad (1)$$

$$\frac{\partial oMn}{\partial t} = -R_{scav} - R_{sink} + \text{advection} + \text{diffusion} \quad (2)$$

213 which include the contribution of rivers (S_{river}), sediment resuspension or non-reductive
 214 dissolution ($S_{sediment}$), atmospheric dust deposition (S_{atm}), dust flux from ice (S_{ice}),
 215 sediment released by ice ($S_{sed\ ice}$), biological uptake and remineralization (S_{bio}), the re-
 216 versible scavenging terms (R_{scav}), and sinking (R_{sink}). The details of the parameteri-
 217 zations are described in the following sections and the parameter values used for the runs
 218 are listed in Table 1.

219 The model was initialized with output from the global Mn model (Van Hulst et
 220 al., 2017) and concentrations are held constant at the sub-domain boundaries. At these
 221 boundaries, the ratio of dissolved to oxidised Mn from the global model were not rep-

Table 1. Constants and parameter values used in the Mn model runs.

Parameter	Description	Value	Source
α_0	Fractional solubility of Mn at 4°C	0.65	Fishwick et al. (2018)
$f_{Mn\ crust}$	Mn fraction in Earth’s crust	527 ppm	Wedepohl (1995)
$f_{Mn\ sed}$	Mn fraction in marine sediment	270 ppm	Macdonald and Gobeil (2012)
m	Molar mass of Mn	54.938 g mol ⁻¹	—
$R_{Mn:N}$	Extended Redfield ratio Mn:N	1.6 : 23,000	Kuss and Kremling (1999)
k_d	Reduction and desorption rate	$4.7 \cdot 10^{-7} \text{ s}^{-1}$	Bruland et al. (1994)
	Photo-enhanced reduction rate	$2.7 \cdot 10^{-5} \text{ s}^{-1}$	Sunda and Huntsman (1994)
k_p	Oxidation and adsorption rate	$7.0 \cdot 10^{-7} \text{ s}^{-1}$	This study ^a
s_{ox}	Sinking rate	0.6 m day ⁻¹	Roy-Barman (2009) / This study
C	Tidal erosion tuning constant	$2.1 \cdot 10^{-6}$	This study
γ	Solubility tuning constant	0.065	This study
R / SPM	River characteristic content		This study ^b
	- Glacial	164 nM / 261 mg L ⁻¹	
	- Continental	30 nM / 12 mg L ⁻¹	
	- Other	2 nM / 4 mg L ⁻¹	

^aUsing data from Colombo et al. (2020, 2022).

^bUsing data from Colombo et al. (2019); Brown et al. (2020).

222 representative (oxidised Mn was too low) and resulted in unusual scavenging behavior. In-
 223 stead, we used dissolved and oxidised Mn concentrations in a band just inside the do-
 224 main (where the model had established normal scavenging behavior) from a test model
 225 run at the end of spin up for the boundary conditions. We conducted sensitivity exper-
 226 iments of the western and northern boundary conditions with enhanced concentrations
 227 to delineate the influence of Pacific water and the transpolar drift on the Canada Basin
 228 (Text S1, Fig. S1-4).

229 **2.2.1 Riverine Source**

230 River discharge contributes Mn to the shelf seas and into the Arctic Ocean (Middag
 231 et al., 2011a). Dissolved Mn is contributed directly in its dissolved form and indirectly
 232 through the dissolution from particle-bound Mn. The contribution of riverine Mn de-
 233 pends on the river discharge, Q , and the concentration in the rivers. These concentra-
 234 tions vary based on properties of the river’s catchment basin: glacial rivers are strongly
 235 enriched in dissolved Mn, continental rivers are somewhat enriched, and in all other rivers,
 236 Mn is not significantly enriched (Colombo et al., 2019). At each time step, the rivers con-
 237 tribute dissolved Mn following:

$$S_{river} = \frac{\overbrace{Q}^{\text{dissolved Mn}}}{\rho_0 \Delta z_{surface}} R_{class} + \beta \frac{\overbrace{Q \cdot SPM_{class} \cdot \alpha_0 \cdot f_{Mn, crust}}^{\text{particle origin dissolved Mn}}}{\rho_0 \Delta z_{surface} m} \quad (3)$$

238 where ρ_0 is the density of the river water, $\Delta z_{surface}$ is the surface grid box thickness,
 239 β is a factor which ranges from 0-1 in our experiments (not tuned, but tested in the up-
 240 per bound river experiment), $f_{Mn, crust}$ is the crustal abundance of Mn, m is the mo-
 241 lar mass of Mn, and α_0 is the fractional solubility of Mn. We use an average value for
 242 the fractional solubility (65%) measured in seawater at 4°C, since this lower tempera-
 243 ture better reflects the CAA (Fishwick et al., 2018). This fractional solubility falls within
 244 the range measured in samples across the world (Fishwick et al., 2018). Each river is as-
 245 signed a class with an associated characteristic trace metal concentration, R_{class} , and
 246 suspended particulate matter content, SPM_{class} , based on catchment basin properties:
 247 glacial, continental, and other (Fig. 3 and Table 1). The Mn concentrations and SPM
 248 content associated with the classes are determined from rivers sampled in the CAA (Colombo
 249 et al., 2019; Brown et al., 2020).

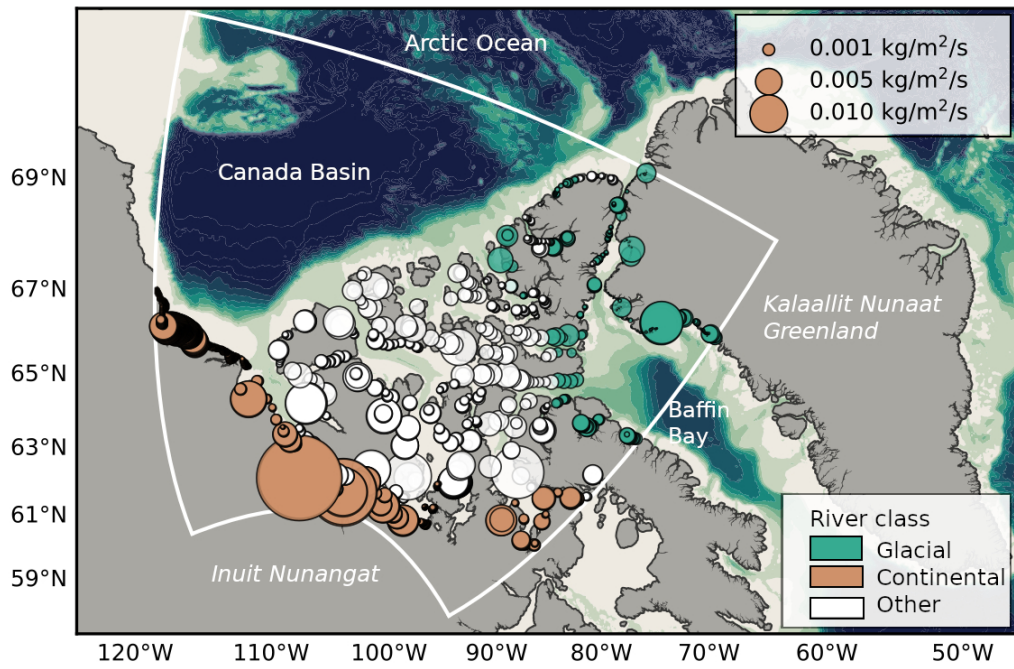


Figure 3. Model rivers were classified based on their drainage basin properties: glacial (green), continental (orange), or other (white). The points on this map are the locations of the river water input in the model and their sizes are proportional to the river discharge in September, 2015 (forcing is repeated from year 2010). Note that the river freshwater flux is remapped to prevent negative model salinities, hence some large rivers are represented as single point sources, while others such as the Mackenzie River consist of multiple point sources along the coastline (Hu et al., 2019).

250 **2.2.2 Atmospheric Aerosol Flux and Release from Sea Ice**

251 Atmospheric aerosols contribute Mn to the ocean through direct deposition to sur-
 252 face waters, Φ_{atm} , or through the deposition onto sea ice and the subsequent release dur-
 253 ing melt, Φ_{ice} . We parameterized these particulate contributions to dMn as:

$$S_{atm\ or\ ice} = \frac{\alpha_0 \cdot f_{Mn\ crust}}{m \cdot \Delta z_{surface}} \cdot \Phi_{atm\ or\ ice} \quad (4)$$

254 The atmospheric and sea ice flux terms are derived from monthly Community Earth Sys-
 255 tem Model (CESM) results. The combined monthly dry and wet atmospheric deposi-
 256 tion fluxes originate from historical (1920-2005) and future (2006-2080) runs of the Com-
 257 munity Atmosphere Model with Chemistry (CAM-Chem) downloaded from the Climate
 258 Data Gateway (CESM1 CAM5 BGC Large Ensemble Atmosphere Post Processed Data;
 259 Tilmes et al., 2016). We estimate tracer fluxes from ice using the monthly Community
 260 Ice CodE ensemble results (CICE; Holland et al., 2012; Kay et al., 2015). These ensem-
 261 ble run sets have a horizontal atmospheric resolution of $0.9 \times 2.5^\circ$ and ocean/ice reso-
 262 lution of $1.6 \times 2.5^\circ$ which we linearly interpolated to the ANHA12 grid. We do not tune
 263 any of the parameters in this process.

264 **2.2.3 Sediment Resuspension over the Continental Shelf**

265 Dissolved Mn increases near the ocean floor in the Canadian Arctic by sediment
 266 resuspension (non-reductive dissolution; Colombo et al., 2020). While reductive disso-
 267 lution is important over the Chukchi Shelf regions (Vieira et al., 2019), we did not in-
 268 clude sediment diffusion as reducing conditions in the sediments are not prevalent in the
 269 CAA (Colombo et al., 2021; Lehmann et al., 2022). Sediment resuspension occurs in-
 270 termittently; Mn integrates the resuspension events and thereby provides a cumulative
 271 view of its prevalence. We incorporated the contribution from sediment resuspension to
 272 dMn as a continuous process:

$$S_{sediment} = \Phi_{erosion} \cdot \frac{\alpha \cdot f_{Mn\ sed}}{m \cdot \Delta z_{bottom}} \quad (5)$$

273 where $f_{Mn\ sed}$ is the fraction of Mn in the particle phase in marine sediments. This frac-
 274 tion is likely to be lower than measured in the continental crust, i.e. Wedepohl (1995),
 275 since it's undergone some amount of chemical transformation. We used the Mn fraction
 276 estimated by Macdonald and Gobeil (2012) from sediments in cores on the shelf and slopes
 277 surrounding the Canada Basin. In Eqn. 5, $\Phi_{erosion}$ is the “erosion ability” (see Fig. S5

278 for the forcing field). This term incorporates the spatial differences in dynamics within
 279 the CAA. West of Barrow Sill, the system has lower mixing rates (Hughes et al., 2018)
 280 and tidal speeds (Epstein, 2018), than the region east of Barrow Sill and around the cen-
 281 tral sills area. These differences impact the sediment resuspension rates, apparent in the
 282 much stronger near-bottom increases of observed dMn in the eastern CAA (Colombo et
 283 al., 2020). We estimate the ability of sediment to be eroded with the barotropic tidal
 284 speed, U_{tidal} , and a tuning constant, C :

$$\Phi_{erosion} = C \cdot U_{tidal}^2 \quad (6)$$

285 The barotropic tidal speeds are from the MOG2D-G model (Carrère & Lyard, 2003) and
 286 are significantly higher in the eastern CAA, compared to the western CAA (Epstein, 2018).
 287 Locations where the tidal speeds are less than 1 cm s^{-1} are masked, since they are be-
 288 low a critical threshold for motion for particles greater than 0.1 mm, i.e. sand. In ar-
 289 eas where resuspension occurs frequently, the easily accessible Mn on particles has al-
 290 ready been removed, resulting in a lower solubility. We reduce the fractional solubility
 291 in Eqn. 5 at high tidal speeds according to:

$$\alpha = \alpha_0 \cdot \frac{\gamma(1 - e^{-U_{tidal}^2/\gamma})}{U_{tidal}^2} \quad (7)$$

292 where γ is a tuning parameter. At small tidal speeds, Eqn. 7 approaches α_0 while at tidal
 293 speeds greater than 0.1 m s^{-1} , fractional solubility decreases and the overall resuspen-
 294 sion rate approaches a constant $\alpha_0\gamma C$ (Fig. S6). The tuning parameters were estimated
 295 based on model behaviour in several tuning runs (see Section 2.3).

296 **2.2.4 Sediment Entrained in Sea Ice and Subsequent Melt**

297 Sediment entrained in sea ice has been identified as an important source of reac-
 298 tive trace metals such as aluminum and iron in the ocean, and thus may also be impor-
 299 tant for Mn (Measures, 1999). In order to parameterize this contribution to dMn, we cou-
 300 ple the Mn contained in sediments in sea ice and the sea ice melt rate, I_{melt} :

$$S_{sed\ ice} = \frac{\alpha_0 \cdot f_{Mn\ sed}}{m \cdot \Delta z_{surface}} \cdot S_p \cdot I_{melt} \quad (8)$$

301 where S_p is the sediment content in sea ice at each grid point. The sediment content is
 302 spatially variable, and depends on the amount of sediment that was incorporated dur-
 303 ing ice formation on the shelves and on sea ice transport. Mn from the sediments dis-
 304 solves with fractional solubility, α_0 , and subsequently undergoes redox cycling and sink-
 305 ing as elsewhere within the water column. Sea ice also contains dissolved Mn, however

306 this component drains out with the brine during early melt (Domena, 2017), and is likely
 307 removed within the first melt season. Hence, we did not consider the dissolved Mn in
 308 sea ice brine fraction in our model.

309 Through particle tracking experiments with Ocean Parcels (Lange & Van Sebille,
 310 2017), we estimated the contribution of sea ice formed over the Siberian shelves during
 311 the stormy fall months (September-December) to the ice in the Canada Basin (Fig. 4).
 312 We released parcels every month over the course of a year and traced them backwards
 313 for three years (the average sea ice age in the Canada Basin and the northwestern CAA
 314 based on satellite information). Almost 40% of the sea ice tracks in the northwestern CAA
 315 and Canada Basin region originated from the Siberian shelves via the transpolar drift
 316 during the fall months, when strong sediment resuspension events coincide with sea ice
 317 formation. The rest of the tracks transit this region during other times of year, circu-
 318 late within the central Canada Basin during the three years of tracking, or originate from
 319 the outer Siberian shelf or Chukchi Sea. The results of the particle tracking experiments
 320 were interpolated and smoothed to create a forcing field which incorporates the spatial
 321 variation in sediment content in sea ice (Fig. S7). In addition, we assumed a low back-
 322 ground value of shelf sediments in sea ice in the CAA. We multiply this forcing field by
 323 a tuned constant, 0.85 kg m^{-3} , which reflects the sediment content of the ice if it were
 324 fully formed over the Siberian shelf in the fall, i.e. the proportion of Siberian tracks was
 325 one.

326 ***2.2.5 Uptake and Remineralization***

327 Dissolved Mn is taken up by phytoplankton in the euphotic zone and is subsequently
 328 remineralized below the euphotic zone. We can quantify this particulate contribution to
 329 dMn by pairing the addition and removal of Mn to the uptake and remineralization of
 330 nitrate:

$$S_{bio} = R_{Mn:N} \cdot \Delta N \quad (9)$$

331 where $R_{Mn:N}$ is the extended Redfield ratio for Mn to nitrogen based on observations
 332 in the North Atlantic (23,000 N : 1.6 Mn; Kuss & Kremling, 1999), and ΔN is the month-
 333 to-month change in nitrate concentration during the summer months (April-August) from
 334 2002-2015 derived from the Canadian Ocean Ecosystem Model (CanOE; Hayashida et
 335 al., 2019). The North Atlantic nutrient balance is strongly influenced by Arctic Ocean

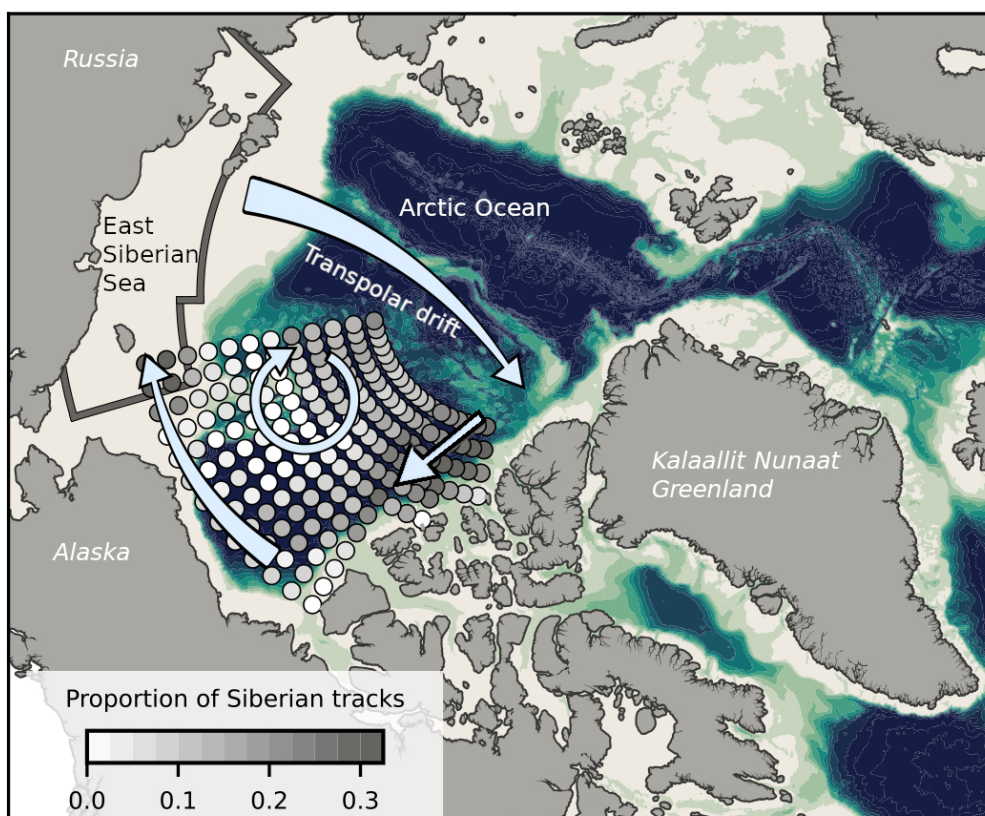


Figure 4. Sediment rich sea ice, produced over the Siberian shelves (East Siberian Sea; region definition outlined in gray) in the fall, is transported across the Arctic Ocean via the transpolar drift. From there it is found predominantly along the outer edges of the Beaufort Gyre; the largest contribution occurs in the northeastern CAA. Ice motion patterns are indicated with light blue arrows. For locations in the Canada Basin, the proportion of parcels traced back to the Siberian shelves (region defined with the brown outline) in the fall months are shown.

336 outflow (Yamamoto-Kawai et al., 2006) and may thus be representative of the CAA. The
 337 Mn:N ratio could be lower in the Arctic Ocean, in which case we slightly underestimate
 338 uptake and remineralization. We assume that the month-to-month change in nitrate is
 339 zero during seasons with low biological activity to avoid confusing the replenishment of
 340 nitrate via mixing with remineralization at the surface. We did not tune the uptake and
 341 remineralization.

342 **2.2.6 Reversible Scavenging and Sinking**

343 Dissolved Mn oxidizes forming larger aggregates and adsorbs to particle surfaces.
 344 dMn is regenerated by the reduction of oxidised Mn and desorption from particles. Since
 345 we do not directly model particle-bound Mn, but rather incorporate its effect on dMn
 346 through dissolution from the source components, we calculate the reversible scavenging
 347 based on the dissolved and oxidised Mn concentrations (Van Hulst et al., 2017):

$$R_{scav} = -k_p \cdot [dMn] + k_d \cdot [oMn] \quad (10)$$

348 where k_p is the adsorption and oxidation rate, and k_d is the desorption and reduction
 349 rate (see Text S2 for the full derivation). The R_{scav} term appears with opposing signs
 350 in the dMn and oMn equations (Eqn. 1 and 2). We estimate the rate constant k_p from
 351 observations of dissolved and particulate Mn in the Canadian Arctic (Colombo et al.,
 352 2020, 2022). As this estimate is based on field data, the rate intrinsically incorporates
 353 the impact of abiotic and microbially enhanced oxidation. Assuming steady state, the
 354 ratio of the scavenging rates is equal to the ratio of dissolved to particulate Mn concen-
 355 trations. This assumption reduces the available observations to those far away from sources
 356 and sinks, i.e. deep stations in Baffin Bay and the Canada Basin (Fig. S8). The ratio
 357 of scavenging rates, k_p/k_d , is estimated as 1.47 ± 0.25 and with a k_d of $4.7 \cdot 10^{-7} \text{ s}^{-1}$
 358 (Bruland et al., 1994), k_p is estimated as $7.0 \cdot 10^{-7} \text{ s}^{-1}$ (Fig. S9). The reduction rate,
 359 k_d , increases from the base rate up to $2.7 \cdot 10^{-5} \text{ s}^{-1}$ in the euphotic zone (photo-enhanced
 360 reduction; Sunda & Huntsman, 1994), proportional to the solar flux that penetrates into
 361 the ocean at the surface, limited by the ice cover (from ANHA12). We estimate the eu-
 362 photic zone depth as 70 m in the Canada Basin with a gradual transition to 50 m in the
 363 CAA (Fig. S10) based on estimates by Bhatia et al. (2021) and Laney et al. (2017); the
 364 euphotic zone depth estimate does not account for sea ice cover. The scavenging rates
 365 in the model do not depend on the dissolved oxygen concentration since Arctic waters
 366 are generally well oxygenated.

367 The oxidised Mn aggregates sink, R_{sink} , and are removed through burial as in Van
 368 Hulten et al. (2017):

$$R_{sink} = s_{ox} \frac{\partial[oMn]}{\partial z} \quad (11)$$

369 where s_{ox} is the sinking rate. The sinking rate was based on the estimate by Roy-Barman
 370 (2009) of 0.4 m d⁻¹ in the interior of the Arctic Ocean and then increased to 0.6 m d⁻¹
 371 based on an evaluation of modelled background oMn concentrations in the Canada Basin
 372 far away from sources and sinks.

373 2.3 Tuning

374 Of the parameters in our model (Table 1), we tuned the oMn sinking rate, sedi-
 375 ment resuspension rate, sediment solubility parameter, and the sediment content in sea
 376 ice (in that order). Below, we describe our choice of criteria and approaches for tuning
 377 these parameters, and compare the parameter values with observations.

378 The sinking rate sets the background oMn (and through reduction, dMn) concen-
 379 trations in regions far away from sources such as deep parts of the Canada Basin. We
 380 initialized the sinking rate in our model as 0.4 m d⁻¹ based on a sinking rate derived
 381 by Roy-Barman (2009) from modelled and measured ²³⁰Th profiles in the interior of the
 382 Arctic Ocean. With a sinking rate of 0.4 m d⁻¹, the deep oMn concentrations in the Canada
 383 Basin in the model were overestimated. An increased sinking rate of 0.6 m d⁻¹ gave rea-
 384 sonable background oMn concentrations. The global model of Mn uses a sinking rate of
 385 1 m d⁻¹ up to 10 m d⁻¹ to account for loss near hydrothermal vents (Van Hulten et al.,
 386 2017).

387 Our sediment resuspension parameterization incorporates two tuned parameters:
 388 the tidal erosion rate constant, C , and solubility parameter, γ . The tidal erosion rate
 389 controls the background (below about 100 m) and near-bottom dMn concentrations in
 390 shelf areas, so in our domain predominantly the CAA. With observed dMn profiles in
 391 the CAA, we assessed the tidal erosion constant that best represented dMn in the lower
 392 water column with multiple test model runs. The solubility parameter limits the sed-
 393 iment resuspension rate in shelf regions with high tidal speeds, and the most appropri-
 394 ate value was estimated mainly based on comparing modelled dMn with observations
 395 at stations CAA6 and CAA9 (characterized by strong tidal speeds). The resultant sed-
 396 iment resuspension rates in our model range from 0 to 2808 g m⁻² yr⁻¹ (median of re-

397 gions with resuspension is $58 \text{ g m}^{-2} \text{ yr}^{-1}$). Particulate material collected in sediment
398 traps over the Beaufort Shelf from spring 1987 to 1988 contained total dry weight par-
399 ticle fluxes associated with terrigenous input ranging from 10 to $80 \text{ g m}^{-2} \text{ yr}^{-1}$ (O’Brien
400 et al., 2006). The largest particle fluxes occurred during the summer and fall. Our me-
401 dian tuned sediment resuspension rate falls within this range.

402 We tuned the sediment content in sea ice last, as it is the most important param-
403 eter in our study. This parameter affects the surface dMn concentrations primarily in
404 the Canada Basin where sea ice contains a significant proportion of non-local sediments
405 (Fig. 4). We assessed the representation of surface dMn concentrations at stations in the
406 Canada Basin after a few years of spin up using several values of the sediment content
407 in ice parameter. The chosen sediment content in sea ice in the Canada Basin in our model
408 ranges from 0 to 267 g m^{-3} (median is 28 g m^{-3} ; average is 64 g m^{-3}). In observations,
409 the sediment load ranges by several orders of magnitude depending on the location sam-
410 pled, the type of ice, and is highly variable year-to-year (see Table S1 for a non-comprehen-
411 sive list of observed sediment content). In the Beaufort Sea, the observed sediment con-
412 tent in ice cores ranged from 31 to 593 g m^{-3} with an average of 157 g m^{-3} (Reimnitz
413 et al., 1993). Our tuned ice sediment content is smaller, but of a similar order of mag-
414 nitude.

415 2.4 Experimental Design

416 Three numerical experiments were performed with the Mn model, running from
417 2002 to 2019: the reference and “clean” sea ice cases, and a sensitivity experiment for
418 the rivers. An additional experiment was performed from 2002 to 2015 to assess the mag-
419 nitude of the impact of biological uptake and remineralization. The reference run includes
420 all model components except uptake and remineralization, and uses a lower bound es-
421 timate of the river contributions (no particle-bound Mn, $\beta = 0$ in Eqn. 3). The clean
422 sea ice case is the same as the reference run, except that the sea ice does not contain sed-
423 iment (i.e. $S_{sed\ ice} = 0$). In order to bound the riverine influence, we perform a sen-
424 sitivity experiment with a distinctly upper bound riverine estimate ($\beta = 1$ in Eqn. 3),
425 compared to the lower bound estimate from the reference run. The treatment of river-
426 ine Mn introduces uncertainties in the model due to the complex estuarine cycling and
427 the influence of particulate matter on dissolved Mn concentrations. In the “upper bound”

428 river experiment, we include the contribution from riverine sediments on the Mn con-
429 centrations in addition to the dissolved Mn.

430 Each experiment is spun up by repeating the year 2002 three times, before start-
431 ing the full run. The run is considered spun up when the year-to-year change in Mn pro-
432 files is minimal (Fig. S11). Analysis was performed using Python 3 (<https://anaconda.com>)
433 within Jupyter Notebooks with the NumPy, Pandas, SciPy, Matplotlib, Seaborn, scikit-
434 learn, and cmocean packages (Pedregosa et al., 2011; Hunter, 2007; Kluyver et al., 2016;
435 Oliphant, 2006; The Pandas development team, 2020; Thyng et al., 2016; Virtanen et
436 al., 2020; Waskom & the Seaborn development team, 2020).

437 **3 Results**

438 Mn profiles throughout our domain are typical for a scavenged type element: con-
439 centrations are higher near sources with a low and homogeneous background (Fig. 5).
440 The background concentrations are controlled by scavenging, sinking, advection and mix-
441 ing, and the resultant redistribution of materials throughout the water column, while the
442 surface Mn maximum is a result of the contributions from river runoff, sea ice melt, dust
443 deposition, photoreduction, and sediment that is resuspended directly into the polar mixed
444 layer. Sediment resuspension leads to near-bottom increases in some regions.

445 **3.1 Model Evaluation**

446 We evaluate the Mn model by comparing simulated dissolved Mn concentrations
447 in August-September 2009 and 2015 from the reference experiment with measurements
448 collected by the IPY and Canadian GEOTRACES cruises during those time periods (Sim,
449 2018; Colombo et al., 2020, Fig. 5-9). We also show mean polar mixed layer dMn con-
450 centrations alongside observations from the 2015 US GEOTRACES GN01 section (Fig. 9a;
451 Jensen et al., 2020; GEOTRACES Intermediate Data Product Group, 2021). We do not
452 focus on particulate Mn as it is only incorporated into the model to estimate the scav-
453 enging of dMn. Nevertheless, modelled oMn displays the observed variability in the up-
454 per 100 m in the CAA in 2015 well (Fig. S12). Overall, our intention is not to replicate
455 the observations, but to incorporate all the processes that control Mn distributions and
456 to capture observed spatial variation. The observations were not used in initial condi-
457 tions or boundary conditions to allow for an independent evaluation.

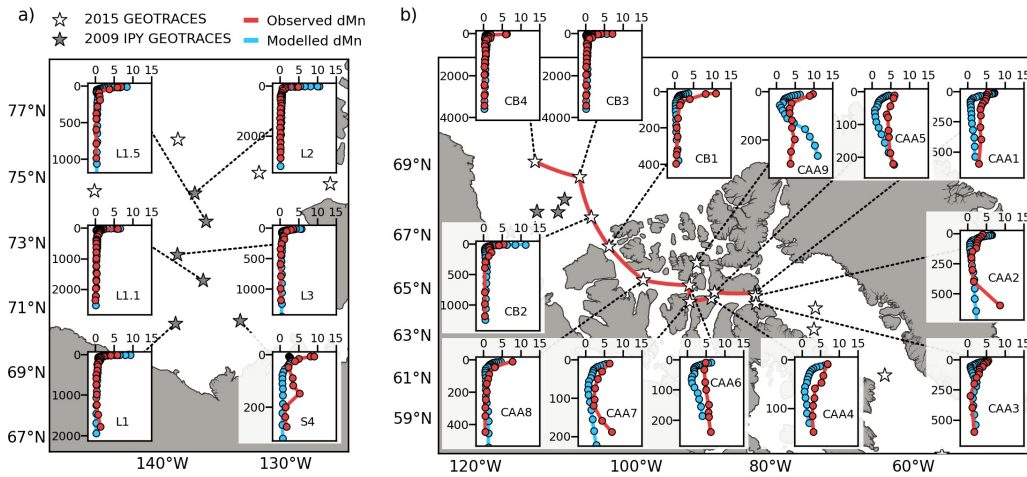


Figure 5. Simulated dissolved Mn profiles (blue) from the reference run compared to observed concentrations (red) from the (a) 2009 IPY GEOTRACES cruise on the Beaufort Shelf and (b) the 2015 Canadian GEOTRACES cruises in the Canadian Arctic Archipelago. Profiles are labelled with station names and their locations are marked with gray (2009 stations) and white (2015 stations) stars. Simulated concentrations were averaged over the time periods of the cruise observations, i.e. August-September. Note that the profile depth (vertical) scales vary.

458 The model captures the regional variation of Mn concentrations along a transect
 459 from the deeper Canada Basin into the shallow CAA (Fig. 6). Observed surface concen-
 460 trations range from 5-10 nM in the Canada Basin and on the Beaufort Shelf, up to 10-
 461 11 nM at CB1, CAA8, and CAA9, and around 5 nM in the rest of the CAA (Fig. 5 and
 462 6). The representation of the Canada Basin and the Beaufort shelf surface is variable
 463 and dependent on the specific patterns of sea ice melt and the Pacific Water inflow. Over-
 464 all, the model does well in the southern Canada Basin and on the Beaufort Shelf (Fig. 9a).
 465 In the central Canada Basin, modelled concentrations are lower than observed; a reflec-
 466 tion of the lower sediment content in the model sea ice forcing in this portion of the Canada
 467 Basin (Fig. S7). Along the western domain boundary and on the Beaufort Shelf, inflow
 468 of Pacific Water increases Mn concentrations in the model and observations (Fig. 9a, S2).
 469 Surface concentrations are overestimated at L2, L1, and CB2 and underestimated at S4
 470 on the Beaufort shelf, and at stations CB4, CB1, and CAA8 in the western CAA which
 471 receive outflow from the Canada Basin (Fig. 5). Within the CAA, surface concentrations
 472 are overestimated at stations CAA1 and CAA2 in Lancaster Sound where waters from
 473 Baffin Bay recirculate, while on the south side of the Channel at CAA3, the model cap-

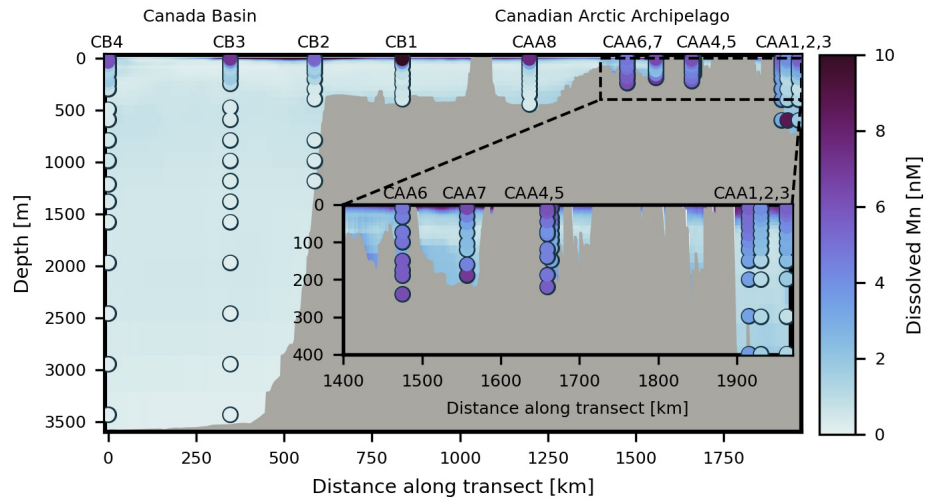


Figure 6. A transect of dissolved Mn concentrations from the Canada Basin through Parry Channel in the Canadian Arctic Archipelago to Baffin Bay (path is shown in red in Fig. 5b). The background shading corresponds to simulated dMn averaged over the sampling time period (August-September, 2015) and the circles indicate observed dMn concentrations from the 2015 GEOTRACES cruises. The inset expands on the Parry Channel region east of Barrow Sill.

474 tures the surface concentrations (Fig. 5). Background concentrations in the model and
 475 observations are low (0-2 nM) in the Canada Basin (0-900 km along the transect in Fig. 6)
 476 and increase (to 1-4 nM) as the waters travel through the shelf areas of the CAA.

477 Within Parry Channel, background concentrations west of Barrow Sill are around
 478 1-2 nM, similar to the Canada Basin, while in the eastern CAA they increase to 3-5 nM
 479 with near-bottom maxima (appear as a slight bend in the modelled Mn profiles in Fig. 5
 480 and Fig. 6). Background concentrations in shallow regions are set by the sediment re-
 481 suspension rate which increases concentrations up to where the surface stratification lim-
 482 its vertical mixing, while within the polar mixed layer concentrations are set by surface
 483 sources. At depths of 40-100 m in the CAA, just below the polar mixed layer, the model
 484 underestimates Mn. Within this depth range, Mn is remineralized, acting as a source
 485 that is not considered in the reference experiment. In the biological experiment, we es-
 486 timate that remineralization accounts for up to 0.3 nM (Fig. S19 and Text S3). At 100-
 487 200 m depth in the Canada Basin and on the Beaufort shelf, observed Mn concentra-
 488 tions are slightly higher than the background concentrations. This increase is associated

489 with the winter Bering Sea Water and is not captured by the model, as it was not rep-
490 resented in the model’s western boundary condition.

491 The net effect of sediment resuspension is well-represented in the background con-
492 centrations, however there are a couple of unusual modelled near-bottom Mn profiles (Fig. 5).
493 At station CAA9 in Penny Strait, the Mn model overestimates background and bottom
494 concentrations by 5 nM. At this station, strong mixing results in constant, “vertical” ob-
495 served Mn profiles (Hughes et al., 2018). Sediment resuspension, based on tidal stress,
496 dominates as a source of Mn to this region. However, this version of the physical model
497 does not incorporate tides. Hence, we add Mn at the bottom, proportional to the strength
498 of tidal stress, without redistributing it due to tidal mixing. At stations CAA2 and CAA7,
499 on the south side of Parry Channel, observed Mn concentrations increase up to 10 nM
500 near the ocean bottom. These peaks in the observations are attributed to sediment re-
501 suspension (Colombo et al., 2020), although the specific mechanism for the strong peak
502 is unclear. The model does not reproduce these local extreme increases, which likely vary
503 on much smaller spatial scales than our parameterizations can resolve. An increase in
504 Mn over the 40 m above the bottom is reproduced by the model at stations CAA2, CAA4,
505 CAA5 and CAA7.

506 While the model is limited in its representation of regions with strongly variable
507 resuspension rates, it performs well within a range of environments: from deep regions
508 in the Canada Basin to shallow areas in the CAA. The model is configured to ask ques-
509 tions about the drivers of Mn variability. It is important to keep in mind that our pa-
510 rameterizations are limited by the spatial and temporal resolution of available informa-
511 tion; small scale variations are unlikely to be captured by the model.

512 **3.2 Importance of Sediment in Sea Ice**

513 In order to evaluate the importance of sea ice and rivers on the representation of
514 Mn in the upper water column (above 50 m), we compare the results of the “clean” sea
515 ice and upper bound river experiments with the reference experiment (Fig. 7). For all
516 experiments, the representation of surface concentrations has a broad spread. The “clean”
517 sea ice experiment underestimates concentrations in the upper water column by several
518 nM (Fig. 7a) and its mean underestimates concentrations by 4 nM. The mean of the ref-
519 erence run, with sediment in sea ice, falls within 1 nM of observed concentrations. The

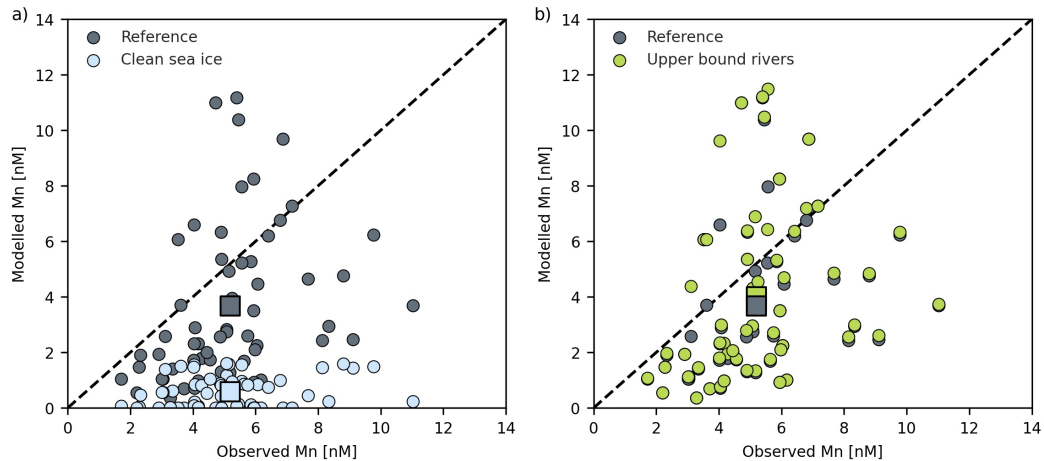


Figure 7. Nearest-depth modelled dMn concentrations compared with observations for depths shallower than 50 m for 2009 IPY and 2015 Canadian GEOTRACES cruises. Square markers indicate the averages of the experiments and observations. (a) The modelled dMn concentrations at the evaluation stations most closely resemble the observations in the reference experiment with sediment in sea ice compared to the “clean” sea ice experiment. Both of these experiments use the lower bound river estimate. (b) The lower and upper bound river experiments, which include sediment within the sea ice, indicate that additional contribution from riverine particulate matter has a relatively small impact.

520 upper bound river experiment slightly increases the surface concentrations relative to
 521 the reference experiment, particularly in the eastern CAA (Fig. 7b). Estimates for sta-
 522 tions in the Canada Basin are unaffected by the addition of particulate matter in rivers.

523 We expect substantial vertical gradients in concentrations in the surface layer in
 524 the Arctic Ocean as a result of the strong stratification. It is difficult to assess the up-
 525 permost modelled concentrations as the shallowest observations are collected at around
 526 10 m below the surface, while the shallowest model estimate is at 0.5 m depth. However,
 527 the Mn-salinity relationship in the model is similar to the observations for the experi-
 528 ment with sediment in sea ice (Fig. S13). In the “clean” sea ice experiment, the model
 529 significantly underestimates the low-salinity Mn endmember.

3.3 Contributions from External Sources of Mn

To assess the relative contributions of each of the external Mn sources, we calculated the annual contribution and flux from these model components in the reference experiment. Our estimate is for the upper 55 m of the water column as we are most interested in the surface layer. An estimate of the full water column differs by including the effects of resuspension in regions deeper than 55 m, thus increasing the importance of resuspension (Table S2). We include estimates from the upper bound river experiment, which does not account for any removal of particulate or dissolved Mn in estuaries, as ranges in the text. We did not include the contributions from (photo)reduction and remineralization as sources of dMn in these calculations since they are part of the internal cycling of Mn. In order to identify regional differences, we separated the domain into the Canada Basin and the Canadian Arctic Archipelago (details in Fig. S14) and subdivided the CAA into west and east along 100°W. Overall, the Canada Basin is more isolated and receives a lower annual contribution of Mn than the CAA: 238-254 versus 370-530 $\mu\text{mol m}^{-2} \text{yr}^{-1}$ (Table 2).

In our model, the dominant source of Mn in the Canada Basin is the release of sediment by sea ice melt (Table 2); it accounts for 87-93% of the average yearly addition of Mn. The amount of melt fluctuates interannually, similar to sea ice area changes observed with satellite data. Nevertheless, from 2002 to 2019, sea ice melt is consistently the largest contributor of Mn in our model in the Canada Basin. Sediment resuspension contributes about 4.4-4.7% in the Canada Basin, mainly over the Beaufort shelf, and river discharge, predominantly from the Mackenzie River, contributes 2.2-8.5%. Atmospheric dust deposited onto the ocean surface, or released during sea ice melt, is not a significant source of Mn anywhere in the domain.

In the CAA, sediment resuspension contributes 40-58% of the annual external addition of Mn to the water column (Table 2). Sediment released by sea ice accounts for 26-37% of Mn; a combination of relatively “clean” sea ice with high melt rates. The river contributions cover a broader range from 5.0-34% in the CAA, compared to 2.2-8.5% in the Canada Basin. Since the total annual Mn addition is greater in the CAA, rivers contribute significantly more dMn to the CAA. Although the Canada Basin receives runoff from the Mackenzie River, the CAA has many rivers of a range of sizes that drain into it, including glacial rivers with high characteristic Mn concentrations.

Table 2. External source contributions to the upper water column of the Canada Basin and the Canadian Arctic Archipelago.^a

Component contribution	Canada Basin		Canadian Arctic Archipelago	
	$\mu\text{mol m}^{-2} \text{ yr}^{-1}$	%	$\mu\text{mol m}^{-2} \text{ yr}^{-1}$	%
River discharge	5.3 (22)	2.2 (8.5)	19 (178)	5.0 (34)
Sediment resuspension	11	4.7 (4.4)	213	58 (40)
Sediment from sea ice	221	93 (87)	138	37 (26)
Dust released by sea ice	0.2	0.1	0.3	0.1
Direct dust deposition	0.0	0.0	0.0	0.0
Total	238 (254)	100	370 (530)	100

^aCalculated as the spatial average annual dissolved Mn contributed by external model source components to the upper 55 m of the water column ($\mu\text{mol m}^{-2} \text{ yr}^{-1}$) in the reference experiment, averaged over the years 2002-2019, separated by region (Fig. S14). Sediment release by sea ice is the only component that varies significantly year-to-year. Estimates from the upper bound river experiment are indicated in parentheses.

Table 3. External source contributions to the upper water column of the western and eastern Canadian Arctic Archipelago.^a

Component contribution	Western CAA		Eastern CAA	
	$\mu\text{mol m}^{-2} \text{ yr}^{-1}$	%	$\mu\text{mol m}^{-2} \text{ yr}^{-1}$	%
River discharge	6.5 (28)	2.2 (8.7)	27 (289)	6.5 (42)
Sediment resuspension	155	52 (49)	256	61 (37)
Sediment from sea ice	136	46 (43)	140	33 (20)
Dust released by sea ice	0.3	0.1	0.3	0.1
Direct dust deposition	0.0	0.0	0.0	0.0
Total	297 (318)	100	424 (686)	100

^aSame as Table 2, except the Canadian Arctic Archipelago (CAA) was subdivided into western and eastern halves along 100°W (near Barrow Sill).

562 Within the CAA, there is a significant difference in dynamical regime west and east
563 of the approximately 120 m deep Barrow Sill (Table 3; Hughes et al., 2017; Colombo et
564 al., 2020, 2021; Q. Wang et al., 2012). The overall contribution of Mn to the water col-
565 umn in the eastern CAA is 424-686 $\mu\text{mol m}^{-2} \text{yr}^{-1}$, compared to 297-318 $\mu\text{mol m}^{-2} \text{yr}^{-1}$
566 in the west. The main contributor to this difference is the 1.6 times stronger sediment
567 resuspension in the eastern CAA. In addition, rivers contribute more strongly to the east-
568 ern CAA relative to the western CAA, 6.5-42% versus 2.2-8.7%, with a broader range
569 in the estimate of their role in the eastern CAA. The eastern CAA receives contributions
570 from the high Mn content glacial rivers that drain Greenland, Ellesmere Island, and Baf-
571 fin Island.

572 Throughout our domain, Mn concentrations are highest in the summer months as
573 a result of seasonally fluctuating components (Fig. 8a). Sea ice melt is largest in July,
574 while the river runoff peak occurs during the freshet in May-June. Due to the large sup-
575 ply of dissolved Mn in the summer months and the increased solar flux, (photo)reduction
576 and oxidation are stronger from July through September. For the month of September,
577 we identified which component on average controls Mn for each horizontal grid cell over
578 the full time series (Fig. 8b). Note that this figure shows where the model adds the con-
579 tribution from a component; where the Mn ends up depends on the advection and dif-
580 fusion of the tracer as well.

581 Within the Canada Basin and portions of the western CAA (the Amundsen Gulf
582 and western Parry Channel), sea ice melt controls the simulated Mn concentrations (Fig. 8b).
583 In the interior of the Beaufort Gyre region, far away from sources and with relatively
584 “clean” sea ice, none of the components contribute significantly. Over the Beaufort Shelf,
585 the Mackenzie River is a regionally important source of Mn; generally river runoff is a
586 significant source at river mouths. In the shallower shelf regions, such as the Beaufort
587 Shelf and the CAA, sediment resuspension is prevalent.

588 The magnitudes of annual Mn fluxes from sources in this Arctic Model (AM; Ta-
589 ble 2) are comparable to those in the first global model of Mn by Van Hulst et al. (2017)
590 (VH). In VH, dust contributes 0-2 $\mu\text{mol m}^{-2} \text{yr}^{-1}$ in the Arctic Ocean, whereas in AM
591 it ranged from 0-0.3 $\mu\text{mol m}^{-2} \text{yr}^{-1}$ (combining direct dust deposition from the atmo-
592 sphere and indirect release from ice). AM riverine fluxes were 5.3-22 $\mu\text{mol m}^{-2} \text{yr}^{-1}$ in
593 the Canada Basin and 19-178 $\mu\text{mol m}^{-2} \text{yr}^{-1}$ in the CAA; higher than the VH estimate

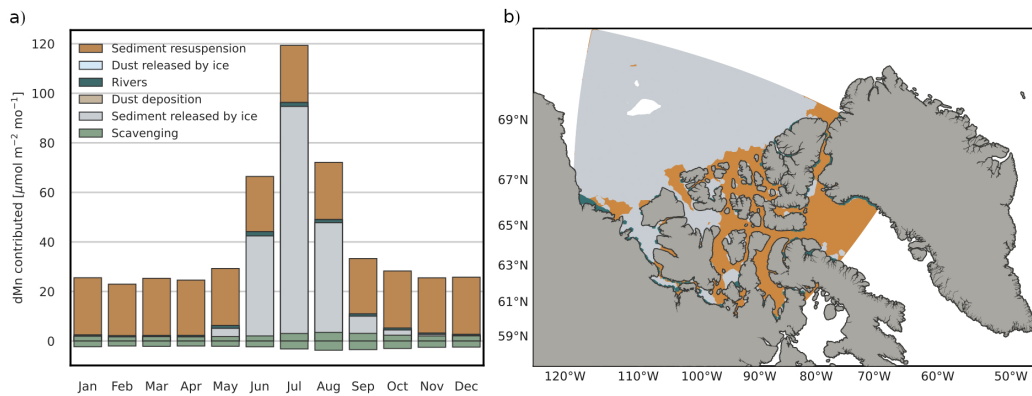


Figure 8. Sediment released by sea ice dominates Mn contributions in the Canada Basin and peaks in July, while sediment resuspension is prevalent over shelf areas including the Canadian Arctic Archipelago. (a) Climatology of the seasonal cycle of Mn contributions for the full water column. The oxidation (removal) and reduction (addition) of Mn through scavenging are calculated as the average through the water column. Sediment resuspension is added at the bottom grid cell, while all other sources act directly on the ocean surface. The contributions from dust deposition and release from ice are too small to appear. (b) Most important Mn contributors to the water column in September based on climatology. At each grid cell, the color represents the most important model forcing component. Places within the model domain where the net contributions are smaller than $0.5 \mu\text{mol m}^{-2} \text{mo}^{-1}$ are white (i.e. in the Canada Basin).

594 of 0-2 $\mu\text{mol m}^{-2} \text{yr}^{-1}$. This range likely reflects a combination of the high Mn content
595 of rivers in the Arctic (Colombo et al., 2019) and alternate treatment of rivers; VH as-
596 sumes a relation between Fe and Mn content, while AM uses observations specific to the
597 Arctic rivers and their catchment basins. In VH, the flux of Mn from bottom sediments
598 in the Arctic Ocean was 5-75 $\mu\text{mol m}^{-2} \text{yr}^{-1}$; AM has 11-213 $\mu\text{mol m}^{-2} \text{yr}^{-1}$. The dif-
599 ference in the upper limit of the range likely reflects the distinctive processes considered
600 by the models: the global model considers sediment diffusion for the flux from sediments,
601 whereas AM considers sediment resuspension because it is more important in the CAA
602 (Colombo et al., 2020). It is also challenging to resolve the large continental shelf regions
603 in the Canadian Arctic in a global model. Lastly, on a global scale, hydrothermal input
604 of Mn at spreading ridges is important (Van Hulst et al., 2017), however we did not
605 include this contribution because the spreading ridges in the Arctic are far away from
606 the AM domain.

607 **3.4 Simulated Surficial Mn During the Summer and the Polar Night**

608 The most significant seasonal and interannual changes in Mn concentrations oc-
609 cur in the polar mixed layer, defined here as the upper 35 m of the water column. For
610 the following characterizations of the simulated concentrations, we will focus on this layer.
611 The upper few meters of the ocean have a strong gradient in Mn concentrations (sim-
612 ulated profile in Fig. S15). It is not possible to measure this layer with conventional meth-
613 ods from a large ship. As such, we exclude the surface 3 m in the results presented here
614 (see Fig. S16 for the surface Mn field) to allow for more direct comparison with exist-
615 ing observations.

616 During summer months, surface Mn concentrations in the Canada Basin mirror the
617 areas of strong sea ice melt and higher sediment content, forming a seasonal Mn max-
618 imum (Fig. 9a, S7). Nearby the western and northern Canada Basin domain boundaries,
619 Pacific Water and transpolar drift water can increase Mn concentrations (Fig. 9a, S2,
620 S4). The highest modelled Mn values are found along the outer edges of the Beaufort
621 Gyre (up to 14 nM). Although rivers contribute only a few percent annually to Mn in
622 the Canada Basin (Table 2), over the continental shelf, plumes of higher Mn concentra-
623 tions extend along coastlines in the summer, starting during the spring freshet (Fig. 9a
624 and Fig. 8b). The plume from the Mackenzie River, the largest river in our domain, ex-
625 tends eastward along the shelf in August, 2015. Glacial drainage is apparent in surface

626 Mn concentrations in a number of coastal regions (Fig. 9a). Along the coast of Green-
627 land, high concentration Mn runoff drains the ice sheet and a number of plumes extend
628 from Nares Strait. In the northern CAA, higher surface concentrations result from a com-
629 bination of sea ice melt and glacial runoff (Fig. 8b). Mn from the Pacific water inflow
630 via the western model boundary influences the Beaufort Shelf but does not significantly
631 affect surface concentrations in the Parry Channel (Text S1, Fig. S2).

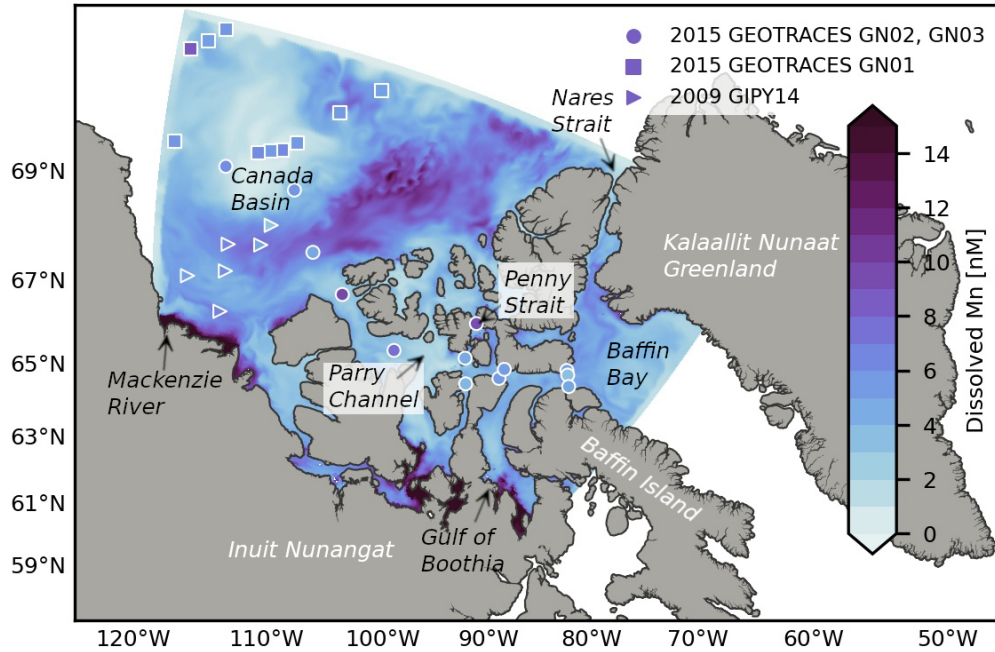
632 Mn concentrations exhibit spatial variability within the CAA (Fig. 9). In west-central
633 CAA, concentrations are low (2-6 nM) and homogeneous. Southern regions, including
634 the Gulf of Boothia, have some of the highest concentrations (8-14+ nM) and flow into
635 the Parry Channel east of Barrow Sill. In this section of central and eastern Parry Chan-
636 nel (and Penny Strait), intermediate concentrations (4-8 nM) are present. In Lancaster
637 Sound, the outflow from Parry Channel follows the southern half of the channel while
638 waters from Baffin Bay (5-8 nM) recirculate along the northern half of Lancaster Sound.
639 Baffin Bay is characterized by lower interior surface concentrations and higher bands as-
640 sociated with Nares Strait and Lancaster Sound outflow.

641 During the Polar Night, fewer sources contribute Mn (Fig. 8a) and there is less spa-
642 tial contrast in surface concentrations (Fig. 9b). Surface concentrations typically range
643 from 1-5 nM, while in the summer they ranged up to 14 nM. The surface Mn maximum
644 is seasonal; by winter, scavenging has removed the relic of summer surface source sig-
645 natures. Regions where Mn is most impacted by sediment resuspension (Fig. 8b), such
646 as the Gulf of Boothia, still have high concentrations in the winter as this component
647 does not vary seasonally.

648 **4 Discussion**

649 In the Arctic Ocean, maximum Mn concentrations occur near the surface in the
650 polar mixed layer and are attributed to freshwater sources such as river discharge and
651 sea ice melt (Campbell & Yeats, 1982; Yeats & Westerlund, 1991; Middag et al., 2011b;
652 Cid et al., 2012; Kondo et al., 2016; Colombo et al., 2020). We present a regional model
653 of Mn in the Canadian Arctic that captures the spatial variability and magnitude of ob-
654 served concentrations. With results from three Mn model experiments (reference, “clean”
655 sea ice, and upper bound river), we identified the dominance of non-local sediment re-
656 leased by sea ice in the Canada Basin, while rivers had a more regional importance. These

a) August



b) January

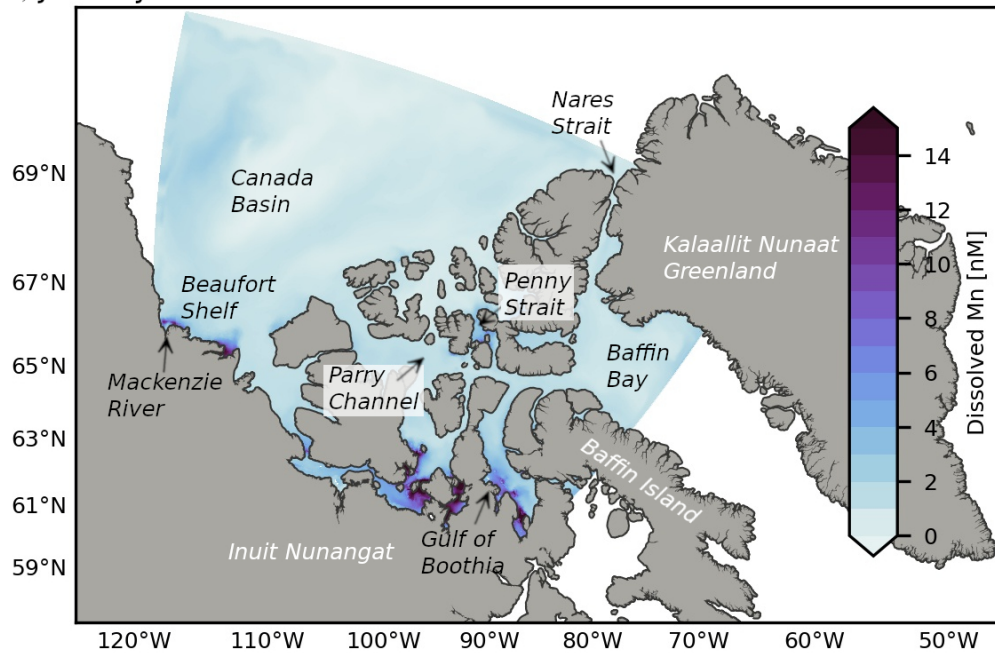


Figure 9. Simulated monthly Mn concentrations in the Polar Mixed Layer, excluding the surface three meters to allow for direct comparison with observations (surface fields in Fig. S16). (a) August, 2015. Markers indicate Polar Mixed Layer dissolved Mn observations from the 2009 GIPY14 and 2015 GEOTRACES GN01, GN02, and GN03 cruises. In the summer, sea ice melt and sediment resuspension dominate the Mn concentrations in the Canada Basin and the Canadian Arctic Archipelago, while freshwater sources such as the Mackenzie River and Greenland meltwater are important regionally. (b) January, 2015. During the Polar night, simulated Mn concentrations are homogeneous and low, however sediment resuspension continues to drive higher concentrations in the south-central CAA.

657 findings suggest that future changes to sea ice transport across the Arctic Ocean may
658 have a significant impact on the supply of Mn and other micronutrients to the Canada
659 Basin and downstream to the CAA.

660 **4.1 Ice-rafted Sediments are the Predominant Source of Mn in the Canada** 661 **Basin**

662 With our model, we found that 87-93% of Mn in the Canada Basin is supplied by
663 sediment from sea ice and 26-37% in the CAA (Table 2). Sediments released by sea ice
664 melt dominate the Mn concentrations in the polar mixed layer during the summer months
665 (Fig. 9a), while in the winter, sea ice blocks the direct surface input of Mn and a lower,
666 more homogeneous distribution results (Fig. 9b). Sediment transport and release by sea
667 ice is the main source of Mn (and likely other similar nutrients) within the Canada Basin,
668 and plays a role within the CAA as well. The majority of sea ice in the interior of the
669 Canada Basin originates from the Siberian shelf regions and traverses the Arctic Ocean
670 via the transpolar drift (Darby, 2003; Eicken et al., 2005; T. Martin & Gerdes, 2007).
671 It spends several years in transit, during which it undergoes freeze-thaw cycles and loses
672 some sediment. The Chukchi Sea may also contribute sea ice to the Canada Basin via
673 the transpolar drift (T. Martin & Gerdes, 2007). In our parameterization, the highest
674 Mn concentrations (and relatively younger ice) are found along the outer edges of the
675 Beaufort Gyre in the Canada Basin, while older ice transported to the interior of the Gyre
676 by convergence has lower Mn concentrations (Fig. 9a). Sea ice formed over the Beau-
677 fort Shelf is transported towards Siberia and does not directly impact the Mn concen-
678 trations in the Canada Basin.

679 Mn sources from the land-ocean interface, such as rivers and sediments, were more
680 important in the CAA than in the Canada Basin, and dynamical differences between the
681 western and eastern CAA translated into distinctive Mn concentrations and component
682 contribution patterns. This separation in dynamics is bounded by the ≈ 120 m deep Bar-
683 row Sill and has been noted in several studies (Hughes et al., 2017; Colombo et al., 2020).
684 In the western CAA, surface concentrations range from 2-6 nM (Fig. 9) and Mn com-
685 ponent contributions share characteristics with the Canada Basin: similar overall river
686 contributions, significant influence from sediments in sea ice, and weaker contributions
687 from sediment resuspension (Table 3). In contrast, in the eastern CAA, Mn concentra-
688 tions are higher (4-8 nM; Fig. 9), sediment resuspension associated with strong tidal speeds

689 dominates, and river discharge plays a more important role. The estimate of the com-
690 ponent contributions is most sensitive in the eastern CAA: the importance of rivers ranges
691 from 6.5% to 42% depending on the treatment of particulate matter. Rivers are preva-
692 lent in the eastern CAA and many of these drain glaciated regions associated with high
693 suspended particulate matter and dissolved Mn. As a result, rivers have the potential
694 to play an important role in the eastern CAA. However, the available information for
695 river input and estuarine removal, limits our ability to constrain the most likely river con-
696 tribution. Based on the surface concentration comparisons (Fig. 7), the upper bound river
697 experiment alters the mean representation slightly; it is inconclusive on the most real-
698 istic representation. The uncertainties associated with these estimates highlight the need
699 for studies on the strength of estuarine removal in the CAA.

700 Eurasian and North American river runoff contribute freshwater to the Arctic Ocean
701 (Proshutinsky et al., 2019; Krishfield et al., 2014) and could contribute Mn to the sur-
702 face maximum. The central Canada Basin contains significant amounts of meteoric wa-
703 ter and sea ice melt (Guay et al., 2009) which feed its freshening (Yamamoto-Kawai et
704 al., 2009). Several studies have looked into the composition of this water. Fichot et al.
705 (2013) did not identify much river runoff in the central basin and Kelly et al. (2019) found
706 that the freshwater contribution from Siberian rivers has decreased since 1997 as a re-
707 sult of the mainly anticyclonic atmospheric circulation pattern over the Canada Basin.
708 Similarly, model trajectories of floats released from Siberian rivers since 1985 do not gen-
709 erally reach the Canada Basin by 2007 (Proshutinsky et al., 2019). In our reference and
710 upper bound river simulations, rivers contribute only 2.2-8.5% to the total budget of Mn
711 in the Canada Basin and 5.0-34% in the CAA (Table 2). However, freshwater sources
712 such as the Mackenzie River on the Beaufort shelf and glacial melt off the coast of Green-
713 land (Fig. 9a) are dominant near coastlines. Inflow from the central Arctic Ocean includ-
714 ing Eurasian runoff enters our study domain through the northern model boundary (Fig. 1).
715 A sensitivity experiment with the northern boundary condition (described in Text S1,
716 boundary condition shown in Fig. S3) indicates weak impact of central Arctic Ocean in-
717 flow on dMn concentrations in the central Canada Basin (Fig. S4). Thus, North Amer-
718 ican river runoff and inflow of Eurasian runoff from the central Arctic Ocean are unlikely
719 to significantly contribute to the freshwater-associated surface Mn maximum in the cen-
720 tral Canada Basin.

721 Nutrient-rich and relatively fresh Pacific water inflow from the Bering Strait is an-
722 other potential source of Mn to the freshwater surface maximum. Pacific Water is trans-
723 ported by the Alaskan Coastal Current along the North American continental shelf. In
724 our domain, the Alaskan Coastal Current enters through the western boundary. An ex-
725 periment with enhanced Mn concentrations in the western boundary condition (Text S1,
726 Fig. S1) indicates that the Pacific Water surface influence is restricted to the Beaufort
727 Shelf and does not affect the Canada Basin interior (Fig. S2). The supply of Pacific Wa-
728 ter from Bering Strait to the Canada Basin is affected by the atmospheric circulation
729 in the Canada Basin (Kelly et al., 2019) and floats released from Bering Strait since 2000
730 also did not enter the central Canada Basin by 2012 (Proshutinsky et al., 2019). It is
731 important to note that our simulated profiles (Fig. 5) do not capture the subtle increase
732 in Mn concentrations associated with the winter Bering Sea Water around 100-200 m
733 depth in the Canada Basin and on the Beaufort Shelf. This limitation is likely because
734 our western boundary condition does not fully capture the higher concentrations of Mn
735 found in the Alaskan Coastal Current and in waters from the Chukchi Shelf. However,
736 the deeper winter Bering Sea Water layer is isolated from the surface through stratifi-
737 cation and does not impact surface Mn concentrations in the Canada Basin (Colombo
738 et al., 2020).

739 In order to assess whether we overestimated the sediment content of sea ice, we per-
740 formed an experiment with “clean” sea ice. In the “clean” ice experiment, the surface
741 Mn concentrations are underestimated by 4 nmol L^{-1} relative to observations (Fig. 7a).
742 If we assume that all of the missing Mn comes from sediment and that Mn added at the
743 surface mixes down to the turbocline, we miss a source that supplies 13-213 grams of sed-
744 iment per squared meter to the surface ocean across the Canada Basin (range based on
745 model turbocline depths in 2015). The magnitude of this component is similar to the
746 average sediment load measured in sea ice cores (Reimnitz et al., 1993; Stierle & Eicken,
747 2002; Eicken et al., 2005). Rivers would be unable to contribute the total amount miss-
748 ing since it must occur over a large area and since the upper bound river experiment shows
749 that additional contributions from rivers do not significantly affect the Canada Basin or
750 the overall surface representation (Fig. 7b, Table 2). In the “clean” sea ice experiment,
751 the freshwater endmember of Mn is also underestimated (Fig. S13). The modelled Mn-
752 salinity relationship is most similar to observations in the experiment with sediment con-
753 tained in sea ice and is comparable with other central Arctic Ocean observations (Middag

754 et al., 2011b). The reference experiment also better reproduces regional differences in
755 the Mn-salinity relationship between the Canada Basin and the CAA.

756 Our results demonstrate that the long range transport of sediments by sea ice from
757 the Siberian shelves is an important source of Mn in the Canada Basin and the Cana-
758 dian Arctic Archipelago. These findings provide support for the sea ice trace metal trans-
759 port mechanism proposed by Measures (1999). Measures (1999) found that the highest
760 Al and Fe concentrations in the central Arctic Ocean coincided with areas with high con-
761 centrations of ice-rafted sediments, instead of river input, and so they hypothesized that
762 transport of ice rafted sediments and the subsequent seasonal melt supplies reactive el-
763 ements to the surface Arctic Ocean. However, their data set did not allow the quantifi-
764 cation of annual fluxes of material to the central Arctic Ocean and so they were unable
765 to quantify the exact contribution of this component to the observed trace metal con-
766 centrations.

767 **4.2 Declining Long Range Sea Ice Transport Could Reduce the Canada** 768 **Basin and Canadian Arctic Archipelago Nutrient Supply**

769 Based on the importance of non-local sediments transported by sea ice (particu-
770 larly from the Siberian shelves), the distributions of trace metals, nutrients, and their
771 biogeochemical cycles in the Arctic basins are likely to be significantly impacted by cli-
772 mate change associated reductions in sea ice. Rising oceanic and atmospheric temper-
773 atures delay the freeze-up period and induce earlier melt of sea ice (Stroeve et al., 2012;
774 Stroeve & Notz, 2018). In addition, in the relatively “quiet” dynamics of the Arctic Ocean,
775 increased mixing may bring warmer Atlantic water (or Pacific Water; Kodaira et al., 2020)
776 to the surface and further increase sea ice melt (D’Asaro & Morison, 1992; Liang & Losch,
777 2018). These factors may significantly reduce the amount of first-year ice that survives
778 in the Kara Sea, East Siberian sea, and western Laptev Sea (Krumpfen et al., 2019).

779 Studies of the transpolar ice drift indicate an increase in drift speed associated with
780 a thinning ice cover and as a result, an increase in exchange of ice-rafted material be-
781 tween regions (Spren et al., 2011; Kwok et al., 2013; Newton et al., 2017; Kipp et al.,
782 2018). However, in recent years, summer ice extents have been small enough in the marginal
783 ice zones, that most of the ice exported from shelves melts before it enters the transpo-

lar drift (Krumpen et al., 2019). These findings suggest a reduction in the transport of matter towards the central Arctic Ocean and Fram Strait by the transpolar ice drift.

In our study, we saw a steady increase in the Mn content of the Canada Basin polar mixed layer from 2002-2019 (Fig. 10), and the primary source of this Mn is sea ice melt (correlation R-squared of 0.97). Note that our experiments do not account for interannual changes in sea ice supply regions. The addition of Mn by melt in our model mirrors satellite observations of sea ice loss in the Beaufort Sea (Fig. 10; correlation R-squared of 0.54). Whereas in the short term, there may be an increase in nutrients supplied by sea ice into the Canada Basin through increased sea ice exchange and melt volume, in the long run, we expect a decrease in supply of sediment rich sea ice from the Siberian shelves via the transpolar drift and a subsequent decline in the surface maximum of Mn in the Canada Basin. Confounding this is the likely increase in transport of riverine and shelf-derived trace elements in the ocean by the transpolar drift as a result of an intensification of the Arctic hydrological cycle and permafrost degradation (Charette et al., 2020).

A reduction in micronutrient supply to the Canada Basin may also have an impact downstream in Baffin Bay. With our experiments, we calculated the transport of Mn through Parry Channel and the contribution of sediment released by sea ice melt to this transport (see Text S4 for details). About 87% of the net Mn transported into Parry Channel from the Canada Basin is contributed by sediments from sea ice and the rest is associated with other sources such as resuspension and runoff (Fig. S17 and S18). Sea ice contributes around 34% of net Mn transported from Parry Channel into Baffin Bay. The reduction in the contribution of these components does not indicate loss in the CAA; it reflects the additional contributions from other sources (mainly sediment resuspension) in the CAA. The sea ice contribution in the water column is significant downstream. However, it is important to note that the sea ice transport in the CAA in the ocean-ice model is stronger than observed due to the lack of a land-fast ice parameterization (Grivault et al., 2018). As a result, we may overestimate the sea ice transport and thus melt in Parry Channel, particularly for the outflow from Parry Channel into Baffin Bay. There are also further factors contributing Mn within the CAA which confound this finding. The acceleration of the hydrological cycle and permafrost thaw may increase the contributions of riverine Mn to the CAA; our experiments do not take these changes into account. On the other hand, sea ice melt is associated with an increase in stratification

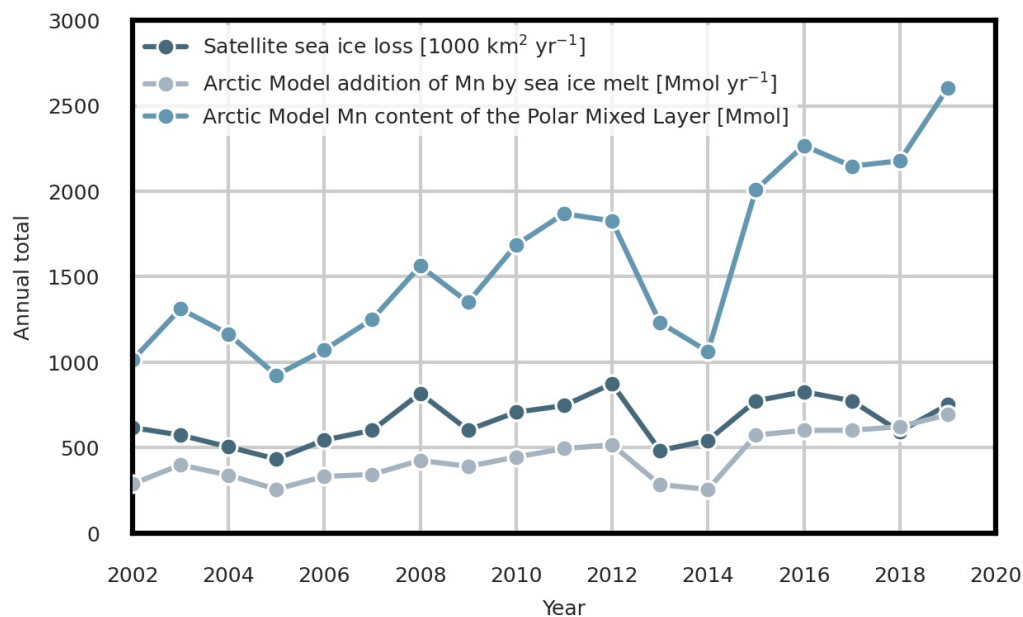


Figure 10. Interannual variations in sea ice melt contribute strongly to Mn supply to the Canada Basin. Conversely, surface Mn concentration changes in the Canada Basin are an indicator of the volume of sediments released by sea ice melt. Sea ice loss is calculated from regional monthly sea ice area changes in the Beaufort Sea measured by the Defense Meteorological Satellite Program series of passive microwave remote sensing instruments (Fetterer et al., 2017). The regional Mn model presented in this study is used to calculate Mn added by sea ice melt and the total Mn content of the Canada Basin.

817 which may reduce the depth up to which resuspended sediment can mix, reducing the
818 Mn supplied into the upper water column (and productive areas) by sediment resuspen-
819 sion in the CAA. However, reduced sea ice cover is also associated with increased wind-
820 driven mixing.

821 Our findings for Mn in the Arctic have implications for nutrients which share sim-
822 ilar sources. In the Arctic Ocean, iron (Fe) behaves similarly to Mn, although Fe is less
823 soluble than Mn and oxidizes more rapidly (Landing & Bruland, 1987; Colombo et al.,
824 2020; Jensen et al., 2020, for a comprehensive discussion). Fe is an essential micronu-
825 trient and it limits primary productivity in some regions of the ocean, such as the South-
826 ern Ocean, parts of the North Atlantic, and the Pacific Northwest (J. H. Martin & Gor-
827 don, 1988; Hawkings et al., 2014; Tagliabue et al., 2017). Generally, iron is not growth
828 limiting in the Arctic (S. Wang et al., 2014), but there is evidence that Fe is limited in
829 specific regions: on the outer shelf and shelf break in the Bering Sea (Aguilar-Islas et al.,
830 2008), as well as in the Barents Sea and Nansen Basin (Rijkenberg et al., 2018). Past
831 studies have indicated that sea ice contributes to the flux of Fe into the ocean (Measures,
832 1999; Lannuzel et al., 2007; Aguilar-Islas et al., 2008; Kanna et al., 2020). Based on the
833 expected changes to the Mn cycle and supply with sea ice melt over the next decades,
834 the supply of Fe to the Canada Basin may be reduced as well. Meanwhile, the increase
835 in simulated Mn content in the Canada Basin from 2002-2019 due to sea ice melt may
836 also have supplied micronutrients such as Fe and have driven some of the observed in-
837 creased Arctic Ocean primary production (Lewis et al., 2020). Changes to Fe availabil-
838 ity impact the community composition and the timing of the spring phytoplankton bloom
839 (Aguilar-Islas et al., 2008), which in turn has consequences for biological productivity,
840 Arctic ecosystems, and the carbon cycle.

841 **4.3 Limitations of Results**

842 **4.3.1 Mn model evaluation**

843 The upper 100 m of the water column are most important to the key findings of
844 this study. In this zone, the Mn representation is impacted by local sources, photo-enhanced
845 reduction, and the physical model's salinity representation and associated mixing. Be-
846 low, we discuss differences between the model and observations and identify the impacts
847 on our findings.

848 In the CAA, the model underestimates Mn in the subsurface (upper 50 m) result-
849 ing in a strong vertical gradient of Mn, particularly in the central sills region. The phys-
850 ical model represents salinity well within the CAA, however the upper 20 m are slightly
851 too fresh, possibly because of an overestimate in the freshwater transport due to too-mobile
852 sea ice without a land-fast sea ice parameterization (Grivault et al., 2018). Despite this,
853 the Mn-salinity relationship matches observations closely in the reference experiment (Fig. S13a).
854 Increased photo-enhanced reduction could increase subsurface Mn. However, trials with
855 a non-linear coupling between light penetration and sea ice concentration did not sig-
856 nificantly affect the subsurface Mn concentrations. Further, while Mn oxides (oMn) are
857 only modelled for their impact on dMn, oMn concentrations are fairly well-represented
858 within the upper water column in the CAA (Fig. S12). Remineralization of Mn taken
859 up by phytoplankton may also counteract some of the subsurface underestimation. How-
860 ever, we estimated that uptake and remineralization altered dissolved Mn profiles by only
861 up to 0.3 nM (Fig. S19 and Text S3). Hence, we suggest that the subsurface Mn under-
862 estimation is most likely caused by improper distribution of materials in the upper wa-
863 ter column from weaker mixing. Replicating the effect of stronger mixing by redistribut-
864 ing the Mn, the average Mn concentrations are underestimated by 1 nM in the upper
865 50 m, while in the subsurface alone they are underestimated by 3 nM. A similar argu-
866 ment can be made for the near-bottom overestimation of Mn at CAA9; a region known
867 to have strong tidal mixing. If we redistribute the Mn throughout the water column, the
868 modelled concentration is overestimated by 2 nM, compared to 5 nM for the lower wa-
869 ter column alone.

870 In the Canada Basin, the physical model captures the depth of isohalines reason-
871 ably well, however the amount of freshwater in the upper water column is underestimated
872 (Hu et al., 2019). This underestimation may be due to a lower freshwater state in the
873 initial conditions derived from the GLORYS2v3 product, but can more likely be attributed
874 to overestimated sea ice concentration and thickness (and underestimated melt in the
875 model). Despite this, the model represents the overall circulation and characteristics of
876 the Canada Basin. For Mn, this shortcoming complicates the evaluation of the Mn-salinity
877 relationship in the Canada Basin (Fig. S13) and instead, we focused our evaluation on
878 Mn with depth (Fig. 5). The underestimation of sea ice melt does not change the actual
879 component contributions estimated by the Mn model: the net effect of the sea ice com-
880 ponent is a combination of ice melt and sediment content. An increase in ice melt would

881 be counterbalanced by a decrease in sediment richness. The exact spatial variability and
882 content of sediment in sea ice of the forcing field is a rough first order estimate, never-
883 theless it is able to provide us with an estimate of the magnitude of the sediment in sea
884 ice component.

885 **4.3.2 Parameterizations**

886 The findings in this study are limited by the parameterizations for scavenging, sed-
887 iment in sea ice, sediment resuspension, and river runoff. Overall, the model is best con-
888 strained for summer months, the southern CAA, and the Canada Basin due to the avail-
889 ability of observations. Scavenging rates are important throughout the water column and
890 are most likely to affect our results in coastal regions. We assumed steady state to es-
891 timate the adsorption and desorption rates from observations; this assumption is least
892 likely to hold in coastal regions and near the surface where scavenging rates are both im-
893 portant and variable. The oxidation rate was derived from observations specific to the
894 Arctic Ocean environment and is faster than the rate used in Van Hulst et al. (2017).
895 The comparison of the modelled and observed oMn profiles (Fig. S12) suggests that the
896 scavenging rates used in this study are representative. However, the scavenging rates are
897 expected to vary spatially and vertically due to variations in Mn oxidizing microbial com-
898 munities and environmental conditions. No data are currently available to represent these
899 effects. For the sediment released by sea ice, we did not account for variations in trans-
900 port of sediment (and its origin) across the Arctic Ocean over the course of the time se-
901 ries. Sea ice drift patterns vary interannually, and so could the source regions for sed-
902 iment transported to the Canada Basin by sea ice. The sediment content would more
903 accurately be represented as a time dependent variable. The total Mn content in the Canada
904 Basin would increase (decrease) with a higher (lower) sediment content in sea ice, while
905 sediment in sea ice would be more (less) important overall. However, observed sediment
906 sea ice loads range several orders of magnitude by location sampled and properties of
907 the ice, and these fluctuations make it challenging to quantify annual changes in over-
908 all sediment content and path travelled. Similarly, sediment resuspension varies inter-
909 annually and seasonally and may be better represented as a time dependent variable.

910 We do not take into account the contributions from breaking of internal waves, storm
911 generated currents, and surface waves on sediment resuspension and coastal erosion. As
912 a result, we likely underestimate sediment resuspension contributions in some areas, par-

913 ticularly during the summer ice-free period. Our treatment of rivers was simplistic and
914 did not account for the complexity of transformations that occur in the estuarine zone.
915 Our results indicate a lower and upper bound of the river contributions, however we are
916 unable to indicate what the actual contribution is. The upper bound river experiment
917 also indicates the effect of higher characteristic riverine Mn concentrations, such as if we
918 had used Eurasian river Mn content within our domain instead of river observations from
919 the CAA. We did not account for the projected seasonal ranges in riverine Mn concen-
920 trations with discharge (Colombo et al., 2019); the river discharge varies seasonally, but
921 we hold the characteristic Mn concentrations of the rivers constant. This approximation
922 could underestimate the riverine contributions during the spring freshet in coastal ar-
923 eas and is most likely to impact the northern CAA and Greenland coast, where glacial
924 rivers are most important. Recent work has suggested ligand stabilization of riverine dis-
925 solved Fe in the Arctic Ocean, increasing its extent of influence (Charette et al., 2020).
926 However, the cycling of dMn in the Arctic Ocean is largely shaped by its redox cycling
927 instead of organic ligand complexation (Colombo et al., 2020; Jensen et al., 2020).

928 While the numbers presented here should be taken as an estimate of magnitude
929 rather than as exact values, the key results are robust to the uncertainties described above.
930 The only way we were able to close the Mn budget (particularly in the Canada Basin)
931 was by incorporating the sediment in sea ice component. Similarly, the only way to rep-
932 resent the higher concentrations of Mn found in the lower water column at some stations
933 in the CAA was through the sediment resuspension term. While the Mn model presented
934 here is limited in its representation of these processes, it provides a platform to ask ques-
935 tions about the drivers of Mn variability and to perform larger scale estimates of the pro-
936 cesses that contribute Mn to the Arctic Ocean. Satellite-based estimates of the distri-
937 bution and quantity of sediment-laden sea ice such as explored in Waga et al. (2022) could
938 strengthen future predictions. The Mn model accuracy would be improved by more com-
939 prehensive estimates of the scavenging and sediment resuspension rates. Observations
940 of Mn along a transect from an estuary into the ocean would help constrain the river-
941 ine contributions.

942 **5 Conclusions**

943 New trace metal datasets collected in the Arctic Ocean as part of the Canadian GEO-
944 TRACES program have provided an essential base for studying biogeochemical cycling

945 in this unique region. Using in situ observations from Colombo et al. (2020), we devel-
946 oped the first model of Mn in the Canadian Arctic Archipelago and the Canada Basin.
947 With three model experiments using the reference period 2002-2019, we looked at (1)
948 the drivers of Mn distributions in the CAA and the Canada Basin and (2) implications
949 of future sea ice transport changes on the biogeochemical cycles of nutrients in the Arc-
950 tic Ocean.

951 (1) While sediment transport by sea ice is identified as important in the Arctic Ocean
952 (Measures, 1999; Eicken et al., 2005), this mechanism is commonly considered less sig-
953 nificant for Mn than riverine input. However, without the contribution from sediment
954 in sea ice to Mn, we were unable to accurately represent the Mn concentrations in the
955 Canada Basin with our model. Sediments transported in sea ice by the transpolar drift
956 account for up to 93% of the total annual Mn added in the Canada Basin and up to 37%
957 in the CAA, driving Mn surface maxima. These results support the hypothesis that “ice-
958 rafted sediment may be an important transport mechanism for supplying reactive trace
959 elements,” proposed by Measures (1999). Rivers are certainly locally important, but con-
960 tribute only 2.2-8.5% annually in the Canada Basin. Within the CAA, our estimates for
961 river contributions ranged from 5.0% up to 34% in the upper bound river experiment.
962 This broad range is the result of the limited information available regarding estuarine
963 cycling in the Arctic. A clear divide is present in the CAA: west of Barrow Sill, the mean
964 concentrations are lower and the behaviour of Mn is more similar to the Canada Basin,
965 while in the eastern CAA, sediments resuspended by high tidal speeds, as well as many
966 glacial rivers drive higher Mn concentrations.

967 (2) Sea ice transport via the transpolar drift is interrupted by Arctic warming (Kruppen
968 et al., 2019) and the decline in this long range transport could reduce the Canada Basin
969 and the CAA nutrient supply. These changes not only impact the Arctic, but also sub-
970 arctic seas, with up to 34% of the Mn transported from Parry Channel into Baffin Bay
971 added by sea ice melt. Mn behaves similarly to Fe in the Arctic Ocean and both of these
972 micronutrients support phytoplankton growth. The importance of sea ice for nutrient
973 supply to the photic zone in the Canada Basin, as well as downstream, is concerning given
974 the recent changes in the Arctic Ocean sea ice regime (reduced summer minimum ice ex-
975 tent, ice thinning, reduction in multi-year ice extent, and altered drift paths). There are
976 many competing factors that will contribute to changes in the biogeochemical cycles; com-

977 bined model-observation studies are highly valuable to understand the individual con-
 978 tribution of these factors.

979 **Acronyms**

980 **CAA** Canadian Arctic Archipelago

981 **NEMO** Nucleus for European Modelling of the Ocean

982 **ANHA12** Arctic and Northern Hemispheric Atlantic 1/12 degree

983 **LIM2** Louvain-la-Neuve version 2

984 **TOP** Tracers in the Ocean Paradigm

985 **TVD** Total Variance Dissipation scheme

986 **CESM** Community Earth System Model

987 **CAM-Chem** Community Atmosphere Model with Chemistry

988 **Acknowledgments**

989 We thank Marco van Hulst for openly sharing his model code and results, Jacqui-Lee
 990 Epstein for extracting the tidal speeds for the sediment resuspension parameterization,
 991 Nadja Steiner and Hakase Hayashida for sharing CanOE model results, and Genevieve
 992 Parton for helpful discussions regarding sediment resuspension. We'd also like to thank
 993 the two reviewers for their helpful comments. This work was funded by the Natural Sci-
 994 ences and Engineering Council (NSERC) Climate Change and Atmospheric Research Grant:
 995 GEOTRACES (RGPC 433848-12) and VITALS (RGPC 433898), an NSERC Discov-
 996 ery Grant (RGPIN-2016-03865) to SEA, and by the University of British Columbia through
 997 a four year fellowship to BR. Computing resources were provided by Compute Canada
 998 (RRG 2648 RAC 2019, RRG 2969 RAC 2020, RRG 1541 RAC 2021). The model con-
 999 figuration, code, results, and analysis code are archived on FRDR at
 1000 <https://doi.org/10.20383/102.0388>. Analysis code is also available via Github at
 1001 <https://github.com/brogalla/Mn-sea-ice-paper>.

1002 **References**

1003 Aguilar-Islas, A. M., Rember, R. D., Mordy, C. W., & Wu, J. (2008). Sea
 1004 ice-derived dissolved iron and its potential influence on the spring algal
 1005 bloom in the Bering Sea. *Geophysical Research Letters*, *35*(24). doi:

1006 10.1029/2008GL035736

1007 Bacon, S., Marshall, A., Holliday, N. P., Aksenov, Y., & Dye, S. R. (2014). Seasonal
1008 variability of the East Greenland Coastal Current. *Journal of Geophysical Re-*
1009 *search: Oceans*, 119(6), 3967-3987. doi: 10.1002/2013JC009279

1010 Balzer, W. (1982). On the distribution of iron and manganese at the sediment/water
1011 interface: Thermodynamic versus kinetic control. *Geochimica et Cosmochimica*
1012 *Acta*, 46(7), 1153-1161. doi: 10.1016/0016-7037(82)90001-1

1013 Bamber, J., Van Den Broeke, M., Ettema, J., Lenaerts, J., & Rignot, E. (2012).
1014 Recent large increases in freshwater fluxes from Greenland into the North
1015 Atlantic. *Geophysical Research Letters*, 39(19). doi: 10.1029/2012GL052552

1016 Bhatia, M. P., Waterman, S., Burgess, D. O., Williams, P. L., Bundy, R. M., Mel-
1017 lett, T., ... Bertrand, E. M. (2021). Glaciers and Nutrients in the Cana-
1018 dian Arctic Archipelago Marine System. *Global Biogeochemical Cycles*, 35,
1019 e2021GB006976. doi: 10.1029/2021GB006976

1020 Bouillon, S., Morales Maqueda, M. A., Legat, V., & Fichet, T. (2009). An elastic-
1021 viscous-plastic sea ice model formulated on Arakawa B and C grids. *Ocean*
1022 *Modelling*, 27(3-4), 174-184. doi: 10.1016/j.ocemod.2009.01.004

1023 Brand, L. E., Sunda, W. G., & Guillard, R. R. L. (1983). Limitation of marine
1024 phytoplankton reproductive rates by zinc, manganese, and iron. *Limnology and*
1025 *Oceanography*, 28(6), 1182-1198. doi: 10.4319/lo.1983.28.6.1182

1026 Brown, K. A., Williams, W. J., Carmack, E. C., Fiske, G., François, R., McLennan,
1027 D., & Peucker-Ehrenbrink, B. (2020). Geochemistry of small Canadian Arctic
1028 rivers with diverse geological and hydrological settings. *Journal of Geophysical*
1029 *Research: Biogeosciences*, 125(1). doi: 10.1029/2019JG005414

1030 Bruland, K. W., Donat, J. R., & Hutchins, D. A. (1991). Interactive influences
1031 of bioactive trace metals on biological production in oceanic waters. *Limnology*
1032 *and Oceanography*, 36(8), 1555-1577. doi: 10.4319/lo.1991.36.8.1555

1033 Bruland, K. W., Oriens, K. J., & Cowen, J. P. (1994). Reactive trace metals in
1034 the stratified central North Pacific. *Geochimica et Cosmochimica Acta*, 58(15),
1035 3171-3182. doi: 10.1016/0016-7037(94)90044-2

1036 Campbell, J. A., & Yeats, P. A. (1982). The distribution of manganese, iron, nickel,
1037 copper and cadmium in the waters of Baffin Bay and the Canadian Arctic
1038 Archipelago. *Oceanologica Acta*, 5(2), 161-168.

- 1039 Carrère, L., & Lyard, F. (2003). Modeling the barotropic response of the global
1040 ocean to atmospheric wind and pressure forcing-comparisons with observa-
1041 tions. *Geophysical Research Letters*, *30*(6). doi: 10.1029/2002GL016473
- 1042 Charette, M. A., Kipp, L. E., Jensen, L. T., Dabrowski, J. S., Whitmore, L. M.,
1043 Fitzsimmons, J. N., ... others (2020). The Transpolar Drift as a source of
1044 riverine and shelf-derived trace elements to the central Arctic Ocean. *Journal*
1045 *of Geophysical Research: Oceans*, *125*(5). doi: 10.1029/2019jc015920
- 1046 Charette, M. A., Lam, P. J., Lohan, M. C., Kwon, E. Y., Hatje, V., Jeandel, C.,
1047 ... Garcia-Orellana, J. (2016). Coastal ocean and shelf-sea biogeochemical
1048 cycling of trace elements and isotopes: lessons learned from GEOTRACES.
1049 *Philosophical Transactions of the Royal Society A: Mathematical, Physical and*
1050 *Engineering Sciences*, *374*(2081), 20160076. doi: 10.1098/rsta.2016.0076
- 1051 Chelton, D. B., de Szoeke, R. A., Schlax, M. G., El Naggar, K., & Siwertz, N.
1052 (1998). Geographical variability of the first baroclinic Rossby radius of
1053 deformation. *Journal of Physical Oceanography*, *28*(3), 433-460. doi:
1054 10.1175/1520-0485(1998)028%3C0433:GVOTFB%3E2.0.CO;2
- 1055 Cid, A. P., Nakatsuka, S., & Sohrin, Y. (2012). Stoichiometry among bioactive trace
1056 metals in the Chukchi and Beaufort Seas. *Journal of Oceanography*, *68*(6),
1057 985-1001. doi: 10.1007/s10872-012-0150-8
- 1058 Colombo, M., Brown, K. A., De Vera, J., Bergquist, B. A., & Orians, K. J. (2019).
1059 Trace metal geochemistry of remote rivers in the Canadian Arctic Archipelago.
1060 *Chemical Geology*, *525*, 479-491. doi: 10.1016/j.chemgeo.2019.08.006
- 1061 Colombo, M., Jackson, S. L., Cullen, J. T., & Orians, K. J. (2020). Dissolved iron
1062 and manganese in the Canadian Arctic Ocean: on the biogeochemical pro-
1063 cesses controlling their distributions. *Geochimica et Cosmochimica Acta*, *277*,
1064 150-174. doi: 10.1016/j.gca.2020.03.012
- 1065 Colombo, M., Li, J., Rogalla, B., Allen, S. E., & Maldonado, M. T. (2022). Par-
1066 ticulate trace element distributions along the Canadian Arctic GEOTRACES
1067 section: shelf-water interactions, advective transport and contrasting biological
1068 production. *Geochimica et Cosmochimica Acta*, *323*, 183-201.
- 1069 Colombo, M., Rogalla, B., Li, J., Allen, S. E., Orians, K. J., & Maldonado, M. T.
1070 (2021). Canadian Arctic Archipelago Shelf-Ocean Interactions: A Major Iron
1071 Source to Pacific Derived Waters Transiting to the Atlantic. *Global Biogeo-*

- 1072 *chemical Cycles*, 35(10), e2021GB007058. doi: 10.1029/2021GB007058
- 1073 Dai, A., Qian, T., Trenberth, K. E., & Milliman, J. D. (2009). Changes in continen-
1074 tal freshwater discharge from 1948 to 2004. *Journal of Climate*, 22(10), 2773-
1075 2792. doi: 10.1175/2008JCLI2592.1
- 1076 Damm, E., Bauch, D., Krumpen, T., Rabe, B., Korhonen, M., Vinogradova, E., &
1077 Uhlig, C. (2018). The Transpolar Drift conveys methane from the Siberian
1078 Shelf to the central Arctic Ocean. *Scientific Reports*, 8(1), 1-10. doi:
1079 10.1038/s41598-018-22801-z
- 1080 Darby, D. A. (2003). Sources of sediment found in sea ice from the western Arctic
1081 Ocean, new insights into processes of entrainment and drift patterns. *Journal*
1082 *of Geophysical Research: Oceans*, 108(C8). doi: 10.1029/2002JC001350
- 1083 Darby, D. A., Myers, W. B., Jakobsson, M., & Rigor, I. (2011). Modern dirty sea ice
1084 characteristics and sources: The role of anchor ice. *Journal of Geophysical Re-*
1085 *search: Oceans*, 116(9). doi: 10.1029/2010JC006675
- 1086 D'Asaro, E. A., & Morison, J. H. (1992). Internal waves and mixing in the Arc-
1087 tic Ocean. *Deep Sea Research Part I: Oceanographic Research Papers*, 39(2),
1088 S459-S484. doi: 10.1016/S0198-0149(06)80016-6
- 1089 Dethleff, D., & Kuhlmann, G. (2009). Entrainment of fine-grained surface deposits
1090 into new ice in the southwestern Kara Sea, Siberian Arctic. *Continental Shelf*
1091 *Research*, 29(4), 691-701. doi: 10.1016/j.csr.2008.11.009
- 1092 Dethleff, D., & Kuhlmann, G. (2010). Fram Strait sea-ice sediment provinces based
1093 on silt and clay compositions identify Siberian Kara and Laptev seas as main
1094 source regions. *Polar Science*, 29(3). doi: 10.3402/polar.v29i3.6070
- 1095 Dethleff, D., Rachold, V., Tintelnot, M., & Antonow, M. (2000). Sea-ice transport
1096 of riverine particles from the Laptev Sea to Fram Strait based on clay min-
1097 eral studies. *International Journal of Earth Sciences*, 89(3), 496-502. doi:
1098 10.1007/s005310000109
- 1099 Domena, V. (2017). *Trace metals in Arctic fast ice* (Master's thesis, Univer-
1100 sity of Alaska Fairbanks). Retrieved from [https://www.proquest.com/](https://www.proquest.com/dissertations-theses/trace-metals-arctic-fast-ice/docview/1990622990/se-2?accountid=14656)
1101 [dissertations-theses/trace-metals-arctic-fast-ice/docview/](https://www.proquest.com/dissertations-theses/trace-metals-arctic-fast-ice/docview/1990622990/se-2?accountid=14656)
1102 [1990622990/se-2?accountid=14656](https://www.proquest.com/dissertations-theses/trace-metals-arctic-fast-ice/docview/1990622990/se-2?accountid=14656)
- 1103 Drinkwater, K. F., & Harding, G. C. (2001). Effects of the Hudson Strait outflow on
1104 the biology of the Labrador Shelf. *Canadian Journal of Fisheries and Aquatic*

- 1105 *Sciences*, 58(1), 171-184. doi: 10.1139/f00-210
- 1106 Eicken, H., Gradinger, R., Gaylord, A., Mahoney, A., Rigor, I., & Melling, H.
 1107 (2005). Sediment transport by sea ice in the Chukchi and Beaufort Seas:
 1108 Increasing importance due to changing ice conditions? *Deep Sea Re-*
 1109 *search Part II: Topical Studies in Oceanography*, 52, 3281-3302. doi:
 1110 10.1016/j.dsr2.2005.10.006
- 1111 Eicken, H., Kolatschek, J., Freitag, J., Lindemann, F., Kassens, H., & Dmitrenko,
 1112 I. (2000). A key source area and constraints on entrainment for basin-scale
 1113 sediment transport by Arctic sea ice. *Geophysical Research Letters*, 27(13),
 1114 1919-1922. doi: 10.1029/1999GL011132
- 1115 Eicken, H., Reimnitz, E., Alexandrov, V., Martin, T., Kassens, H., & Viehoff,
 1116 T. (1997). Sea-ice processes in the Laptev Sea and their importance
 1117 for sediment export. *Continental Shelf Research*, 17(2), 205-233. doi:
 1118 10.1016/S0278-4343(96)00024-6
- 1119 Epstein, J.-L. (2018). *The impact of internal tide mixing parameterizations in*
 1120 *an eddy-permitting model of the Arctic Ocean* (Master's thesis, University of
 1121 British Columbia). doi: 10.14288/1.0365809
- 1122 Evans, L. K., & Nishioka, J. (2018). Quantitative analysis of Fe, Mn and Cd from
 1123 sea ice and seawater in the Chukchi Sea, Arctic Ocean. *Polar Science*, 17, 50-
 1124 58. doi: 10.1016/j.polar.2018.07.002
- 1125 Fetterer, F., Knowles, K., Meier, W. N., Savoie, M., & Windnagel, A. K. (2017).
 1126 Updated daily: Sea ice index, version 3. Boulder, Colorado USA. *NSIDC:*
 1127 *National Snow and Ice Data Center*. doi: 10.7265/N5K072F8
- 1128 Fichet, T., & Maqueda, M. A. M. (1997). Sensitivity of a global sea ice model
 1129 to the treatment of ice thermodynamics and dynamics. *Journal of Geophysical*
 1130 *Research: Oceans*, 102(C6), 12609-12646. doi: 10.1029/97JC00480
- 1131 Fichot, C. G., Kaiser, K., Hooker, S. B., Amon, R. M., Babin, M., Bélanger, S., . . .
 1132 Benner, R. (2013). Pan-Arctic distributions of continental runoff in the Arctic
 1133 Ocean. *Scientific Reports*, 3(1), 1-6. doi: 10.1038/srep01053
- 1134 Fishwick, M. P., Ussher, S. J., Sedwick, P. N., Lohan, M. C., Worsfold, P. J.,
 1135 Buck, K. N., & Church, T. M. (2018). Impact of surface ocean con-
 1136 ditions and aerosol provenance on the dissolution of aerosol manganese,
 1137 cobalt, nickel and lead in seawater. *Marine Chemistry*, 198, 28-43. doi:

1138 10.1016/J.MARCHEM.2017.11.003

1139 Gent, P. R., Willebrand, J., McDougall, T. J., & McWilliams, J. C. (1995). Param-
1140 eterizing eddy-induced tracer transport in ocean circulation models. *Journal*
1141 *of Physical Oceanography*, *25*(4), 463-474. doi: 10.1175/1520-0485(1995)025%
1142 3C0463:PEITTI%3E2.0.CO;2

1143 GEOTRACES Intermediate Data Product Group. (2021). The GEOTRACES Inter-
1144 mediate Data Product 2021 (IDP2021) [Dataset].
1145 doi: 10.5285/cf2d9ba9-d51d-3b7c-e053-8486abc0f5fd

1146 Granskog, M. A., Kaartokallio, H., & Shirasawa, K. (2003). Nutrient status of
1147 Baltic Sea ice: Evidence for control by snow-ice formation, ice permeabil-
1148 ity, and ice algae. *Journal of Geophysical Research: Oceans*, *108*(C8). doi:
1149 10.1029/2002jc001386

1150 Greene, C. H., & Pershing, A. J. (2007). Climate drives sea change. *Science*,
1151 *315*(5815), 1084-1085. doi: 10.1126/science.1136495

1152 Grivault, N., Hu, X., & Myers, P. G. (2018). Impact of the surface stress on the
1153 volume and freshwater transport through the Canadian Arctic Archipelago
1154 from a high-resolution numerical simulation. *Journal of Geophysical Research:*
1155 *Oceans*, *123*(12), 9038-9060. doi: 10.1029/2018JC013984

1156 Guay, C. K. H., McLaughlin, F. A., & Yamamoto-Kawai, M. (2009). Differen-
1157 tiating fluvial components of upper Canada Basin waters on the basis of
1158 measurements of dissolved barium combined with other physical and chem-
1159 ical tracers. *Journal of Geophysical Research: Oceans*, *114*(C1). doi:
1160 10.1029/2008JC005099

1161 Hawkings, J. R., Wadham, J. L., Tranter, M., Raiswell, R., Benning, L. G.,
1162 Statham, P. J., ... Telling, J. (2014). Ice sheets as a significant source of
1163 highly reactive nanoparticulate iron to the oceans. *Nature Communications*,
1164 *5*(1), 1-8. doi: 10.1038/ncomms4929

1165 Hayashida, H., Christian, J. R., Holdsworth, A. M., Hu, X., Monahan, A. H.,
1166 Mortenson, E., ... Steiner, N. S. (2019). CSIB v1 (Canadian Sea-ice Biogeo-
1167 chemistry): a sea-ice biogeochemical model for the NEMO community ocean
1168 modelling framework. *Geoscientific Model Development*, *12*(5), 1965-1990. doi:
1169 10.5194/gmd-12-1965-2019

- 1170 Hölemann, J., Wegener, A., & Schirmacher, M. (1999). Dissolved and particulate
1171 major and trace elements in newly formed ice from the Laptev Sea (Transdrift
1172 III, October 1995). In *Land-ocean systems in the Siberian Arctic* (p. 101-111).
1173 Springer Berlin Heidelberg. doi: 10.1007/978-3-642-60134-7_11
- 1174 Holland, M. M., Bailey, D. A., Briegleb, B. P., Light, B., & Hunke, E. (2012). Im-
1175 proved sea ice shortwave radiation physics in CCSM4: The impact of melt
1176 ponds and aerosols on Arctic sea ice. *Journal of Climate*, 25(5), 1413-1430.
1177 doi: 10.1175/JCLI-D-11-00078.1
- 1178 Hu, X., Myers, P. G., & Lu, Y. (2019). Pacific water pathway in the Arctic
1179 Ocean and Beaufort Gyre in two simulations with different horizontal reso-
1180 lutions. *Journal of Geophysical Research: Oceans*, 124(8), 6414-6432. doi:
1181 10.1029/2019JC015111
- 1182 Hu, X., Sun, J., Chan, T. O., & Myers, P. G. (2018). Thermodynamic and dy-
1183 namic ice thickness contributions in the Canadian Arctic Archipelago in
1184 NEMO-LIM2 numerical simulations. *The Cryosphere*, 12, 1233-1247. doi:
1185 10.5194/tc-12-1233-2018
- 1186 Hughes, K. G., Klymak, J. M., Hu, X., & Myers, P. G. (2017). Water mass
1187 modification and mixing rates in a 1/12 simulation of the Canadian Arctic
1188 Archipelago. *Journal of Geophysical Research: Oceans*, 122, 803-820. doi:
1189 10.1002/2016JC012235
- 1190 Hughes, K. G., Klymak, J. M., Williams, W. J., & Melling, H. (2018). Tidally mod-
1191 ulated internal hydraulic flow and energetics in the central Canadian Arctic
1192 Archipelago. *Journal of Geophysical Research: Oceans*, 123(8), 5210-5229. doi:
1193 10.1029/2018JC013770
- 1194 Hunter, J. D. (2007). Matplotlib: A 2D graphics environment. *Computing in science
1195 & engineering*, 9(3), 90-95.
- 1196 Jakobsson, M. (2002). Hypsometry and volume of the Arctic Ocean and its con-
1197 stituent seas. *Geochemistry, Geophysics, Geosystems*, 3(5), 1-18. doi: 10.1029/
1198 2001GC000302
- 1199 Jensen, L. T., Morton, P., Twining, B. S., Heller, M. I., Hatta, M., Measures, C. I.,
1200 ... Fitzsimmons, J. N. (2020). A comparison of marine Fe and Mn cycling:
1201 U.S. GEOTRACES GN01 Western Arctic case study. *Geochimica et Cos-
1202 mochimica Acta*. doi: 10.1016/j.gca.2020.08.006

- 1203 Johnson, K. S., Coale, K. H., Berelson, W. M., & Michael Gordon, R. (1996). On
1204 the formation of the manganese maximum in the oxygen minimum. *Geochim-*
1205 *ica et Cosmochimica Acta*, *60*(8), 1291-1299. doi: 10.1016/0016-7037(96)00005
1206 -1
- 1207 Kanna, N., Lannuzel, D., van der Merwe, P., & Nishioka, J. (2020). Size frac-
1208 tionation and bioavailability of iron released from melting sea ice in a
1209 subpolar marginal sea. *Marine Chemistry*, *221*, 103774. doi: 10.1016/
1210 j.marchem.2020.103774
- 1211 Kay, J. E., Deser, C., Phillips, A., Mai, A., Hannay, C., Strand, G., . . . Vertenstein,
1212 M. (2015). The community earth system model (CESM) large ensemble
1213 project : A community resource for studying climate change in the presence of
1214 internal climate variability. *Bulletin of the American Meteorological Society*,
1215 *96*(8), 1333-1349. doi: 10.1175/BAMS-D-13-00255.1
- 1216 Kelly, S. J., Proshutinsky, A., Popova, E. K., Aksenov, Y. K., & Yool, A. (2019). On
1217 the origin of water masses in the Beaufort Gyre. *Journal of Geophysical Re-*
1218 *search: Oceans*, *124*(7), 4696-4709. doi: 10.1029/2019JC015022
- 1219 Kempema, E. W., Reimnitz, E., & Barnes, P. (1989). Sea ice sediment entrain-
1220 ment and rafting in the Arctic. *Journal of Sedimentary Petrology*, *59*(2), 308-
1221 317. doi: 10.1306/212F8F80-2B24-11D7-8648000102C1865D
- 1222 Kipp, L. E., Charette, M. A., Moore, W. S., Henderson, P. B., & Rigor, I. G.
1223 (2018). Increased fluxes of shelf-derived materials to the central Arctic Ocean.
1224 *Science Advances*, *4*(1). doi: 10.1126/sciadv.aao1302
- 1225 Klinkhammer, G. P., & Bender, M. L. (1980). The distribution of manganese in the
1226 Pacific Ocean. *Earth and Planetary Science Letters*, *46*(3), 361-384. doi: 10
1227 .1016/0012-821X(80)90051-5
- 1228 Kluyver, T., Ragan-Kelley, B., Pérez, F., Granger, B., Bussonnier, M., Frederic, J.,
1229 . . . others (2016). *Jupyter Notebooks – a publishing format for reproducible*
1230 *computational workflows* (F. Loizides & B. Schmidt, Eds.). IOS Press.
- 1231 Kodaira, T., Waseda, T., Nose, T., & Inoue, J. (2020). Record high Pacific
1232 Arctic seawater temperatures and delayed sea ice advance in response
1233 to episodic atmospheric blocking. *Scientific Reports*, *10*(1), 1-12. doi:
1234 10.1038/s41598-020-77488-y

- 1235 Kondo, Y., Obata, H., Hioki, N., Ooki, A., Nishino, S., Kikuchi, T., & Kuma, K.
1236 (2016). Transport of trace metals (Mn, Fe, Ni, Zn and Cd) in the western
1237 Arctic Ocean (Chukchi Sea and Canada Basin) in late summer 2012. *Deep*
1238 *Sea Research Part I: Oceanographic Research Papers*, 116, 236-252. doi:
1239 10.1016/J.DSR.2016.08.010
- 1240 Krachler, M., Zheng, J., Fisher, D., & Shotyk, W. (2005). Analytical proce-
1241 dures for improved trace element detection limits in polar ice from Arctic
1242 Canada using ICP-SMS. *Analytica Chimica Acta*, 530(2), 291-298. doi:
1243 10.1016/j.aca.2004.09.024
- 1244 Krishfield, R. A., Proshutinsky, A., Tateyama, K., Williams, W. J., Carmack, E. C.,
1245 McLaughlin, F. A., & Timmermans, M. L. (2014). Deterioration of perennial
1246 sea ice in the Beaufort Gyre from 2003 to 2012 and its impact on the oceanic
1247 freshwater cycle. *Journal of Geophysical Research: Oceans*, 119(2), 1271-1305.
1248 doi: 10.1002/2013JC008999
- 1249 Krumpen, T., Belter, H. J., Boetius, A., Damm, E., Haas, C., Hendricks, S., ...
1250 Stein, R. (2019). Arctic warming interrupts the Transpolar Drift and affects
1251 long-range transport of sea ice and ice-rafted matter. *Scientific Reports*, 9(1),
1252 1-9. doi: 10.1038/s41598-019-41456-y
- 1253 Kuss, J., & Kremling, K. (1999). Spatial variability of particle associated trace
1254 elements in near-surface waters of the North Atlantic (30 N/60 W to 60 N/2
1255 W), derived by large volume sampling. *Marine Chemistry*, 68(1-2), 71-86. doi:
1256 10.1016/S0304-4203(99)00066-3
- 1257 Kwok, R., Spreen, G., & Pang, S. (2013). Arctic sea ice circulation and drift speed:
1258 Decadal trends and ocean currents. *Journal of Geophysical Research: Oceans*,
1259 118(5), 2408-2425. doi: 10.1002/jgrc.20191
- 1260 Landing, W. M., & Bruland, K. W. (1987). The contrasting biogeochemistry of
1261 iron and manganese in the Pacific Ocean. *Geochimica et Cosmochimica Acta*,
1262 51(1), 29-43. doi: 10.1016/0016-7037(87)90004-4
- 1263 Laney, S. R., Krishfield, R. A., & Toole, J. M. (2017, 9). The euphotic zone un-
1264 der Arctic Ocean sea ice: Vertical extents and seasonal trends. *Limnology and*
1265 *Oceanography*, 62, 1910-1934. doi: 10.1002/LNO.10543
- 1266 Lange, M., & Van Sebille, E. (2017). Parcels v0.9: Prototyping a Lagrangian ocean
1267 analysis framework for the petascale age. *Geoscientific Model Development*,

- 1268 10(11), 4175-4186. doi: 10.5194/gmd-10-4175-2017
- 1269 Lannuzel, D., Schoemann, V., de Jong, J., & Tison, J.-L. (2007). Distribution and
1270 biogeochemical behaviour of iron in the East Antarctic sea ice. *Marine Chem-*
1271 *istry*, 106(1-2), 18-32. doi: 10.1016/J.MARCHEM.2006.06.010
- 1272 Lavelle, J. W., Cowen, J. P., & Massoth, G. J. (1992). A model for the deposition
1273 of hydrothermal manganese near ridge crests. *Journal of Geophysical Research*,
1274 97(C5), 7413. doi: 10.1029/92JC00406
- 1275 Lehmann, N., Kienast, M., Granger, J., & Tremblay, J.-É.. (2022). Physical
1276 and Biogeochemical Influences on Nutrients Through the Canadian Arctic
1277 Archipelago: Insights From Nitrate Isotope Ratios. *Journal of Geophysical*
1278 *Research: Oceans*, 127(3), e2021JC018179. doi: 10.1029/2021JC018179
- 1279 Lévy, M., Estublier, A., & Madec, G. (2001). Choice of an advection scheme for bio-
1280 geochemical models. *Geophysical Research Letters*, 28(19), 3725-3728. doi: 10
1281 .1029/2001GL012947
- 1282 Lewis, K. M., van Dijken, G. L., & Arrigo, K. R. (2020). Changes in phytoplankton
1283 concentration now drive increased Arctic Ocean primary production. *Science*,
1284 369(6500), 198-202. doi: 10.1126/science.aay8380
- 1285 Liang, X., & Losch, M. (2018). On the effects of increased vertical mixing on the
1286 Arctic Ocean and sea ice. *Journal of Geophysical Research: Oceans*, 123(12).
1287 doi: 10.1029/2018JC014303
- 1288 Macdonald, R. W., & Gobeil, C. (2012). Manganese sources and sinks in the Arctic
1289 Ocean with reference to periodic enrichments in basin sediments. *Aquatic Geo-*
1290 *chemistry*, 18(6), 565-591. doi: 10.1007/s10498-011-9149-9
- 1291 Madec, G. (2008). NEMO ocean engine. *Note du Pôle de modélisation, Insti-*
1292 *tut Pierre-Simon Laplace*, 27(1288-1619). Retrieved from [https://www.nemo-](https://www.nemo-ocean.eu/wp-content/uploads/NEMO_book.pdf)
1293 [ocean.eu/wp-content/uploads/NEMO_book.pdf](https://www.nemo-ocean.eu/wp-content/uploads/NEMO_book.pdf)
- 1294 Mann, P. J., Spencer, R. G. M., Hernes, P. J., Six, J., Aiken, G. R., Tank, S. E.,
1295 ... Holmes, R. M. (2016). Pan-Arctic trends in terrestrial dissolved organic
1296 matter from optical measurements. *Frontiers in Earth Science*, 4, 25. doi:
1297 10.3389/feart.2016.00025
- 1298 Martin, J. H., & Gordon, R. M. (1988). Northeast Pacific iron distributions in re-
1299 lation to phytoplankton productivity. *Deep Sea Research Part I: Oceanographic*
1300 *Research Papers*, 35(2), 177-196. doi: 10.1016/0198-0149(88)90035-0

- 1301 Martin, T., & Gerdes, R. (2007). Sea ice drift variability in Arctic Ocean Model
1302 Intercomparison Project models and observations. *Journal of Geophysical Re-*
1303 *search: Oceans*, 112(C4). doi: 10.1029/2006JC003617
- 1304 Masina, S., Storto, A., Ferry, N., Valdivieso, M., Haines, K., Balmaseda, M., ...
1305 Parent, L. (2017). An ensemble of eddy-permitting global ocean reanal-
1306 yses from the MyOcean project. *Climate Dynamics*, 49(3), 813-841. doi:
1307 10.1007/s00382-015-2728-5
- 1308 Measures, C. I. (1999). The role of entrained sediments in sea ice in the distribu-
1309 tion of aluminium and iron in the surface waters of the Arctic Ocean. *Marine*
1310 *Chemistry*, 68, 59-70. doi: 10.1016/S0304-4203(99)00065-1
- 1311 Michel, C., Ingram, R. G., & Harris, L. R. (2006, 10). Variability in oceanog-
1312 raphic and ecological processes in the canadian arctic archipelago. *Progress in*
1313 *Oceanography*, 71, 379-401. doi: 10.1016/J.POCEAN.2006.09.006
- 1314 Middag, R., de Baar, H. J. W., Laan, P., Cai, P. H., & van Ooijen, J. C. (2011a).
1315 Dissolved manganese in the Atlantic sector of the Southern Ocean. *Deep Sea*
1316 *Research Part II: Topical Studies in Oceanography*, 58(25-26), 2661-2677. doi:
1317 10.1016/J.DSR2.2010.10.043
- 1318 Middag, R., de Baar, H. J. W., Laan, P., & Klunder, M. B. (2011b). Fluvial and
1319 hydrothermal input of manganese into the Arctic Ocean. *Geochimica et Cos-*
1320 *mochimica Acta*, 75(9), 2393-2408. doi: 10.1016/J.GCA.2011.02.011
- 1321 Newton, R., Pfirman, S., Tremblay, B., & DeRepentigny, P. (2017). Increasing
1322 transnational sea-ice exchange in a changing Arctic Ocean. *Earth's Future*,
1323 5(6), 633-647. doi: 10.1002/2016EF000500
- 1324 Nürnberg, D., Wollenburg, I., Dethleff, D., Eicken, H., Kassens, H., Letzig, T.,
1325 & Reimnitz, E. (1994). Sediments in Arctic sea ice: Implications for en-
1326 trainment, transport and release. *Marine Geology*, 119, 185-214. doi:
1327 10.1016/0025-3227(94)90181-3
- 1328 O'Brien, M. C., Macdonald, R. W., Melling, H., & Iseki, K. (2006). Particle fluxes
1329 and geochemistry on the Canadian Beaufort Shelf: Implications for sediment
1330 transport and deposition. *Continental Shelf Research*, 26(1), 41-81. doi:
1331 10.1016/J.CSR.2005.09.007
- 1332 Oliphant, T. E. (2006). *A guide to NumPy* (Vol. 1). Trelgol Publishing USA.

- 1333 Pedregosa, F., Varoquaux, G., Gramfort, A., Michel, V., Thirion, B., Grisel, O., ...
1334 Duchesnay, E. (2011). Scikit-learn: Machine learning in Python. *Journal of*
1335 *Machine Learning Research*, 12, 2825-2830.
- 1336 Peeken, I., Primpke, S., Beyer, B., Gütermann, J., Katlein, C., Krumpen, T., ...
1337 Gerdts, G. (2018). Arctic sea ice is an important temporal sink and means
1338 of transport for microplastic. *Nature Communications*, 9(1), 1-12. doi:
1339 10.1038/s41467-018-03825-5
- 1340 Pfirman, S. L., Eicken, H., Bauch, D., & Weeks, W. (1995). The potential trans-
1341 port of pollutants by Arctic sea ice. *Science of The Total Environment*, 159(2-
1342 3), 129-146. doi: 10.1016/0048-9697(95)04174-Y
- 1343 Proshutinsky, A., Krishfield, R., Toole, J. M., Timmermans, M. L., Williams, W.,
1344 Zimmermann, S., ... Zhao, J. (2019). Analysis of the Beaufort Gyre freshwa-
1345 ter content in 2003–2018. *Journal of Geophysical Research: Oceans*, 124(12),
1346 9658-9689. doi: 10.1029/2019JC015281
- 1347 Reimnitz, E., McCormick, M., McDougall, K., & Brouwers, E. (1993). Sediment ex-
1348 port by ice rafting from a coastal polynya. *Arctic, Antarctic, and Alpine Re-*
1349 *search*, 25(2), 83-98. doi: 10.1080/00040851.1993.12002988
- 1350 Rijkenberg, M. J. A., Slagter, H. A., van der Loeff, M., van Ooijen, J., & Gerringa,
1351 L. J. A. (2018). Dissolved Fe in the deep and upper Arctic Ocean with a focus
1352 on Fe limitation in the Nansen Basin. *Frontiers in Marine Science*, 5, 88. doi:
1353 10.3389/fmars.2018.00088
- 1354 Roy-Barman, M. (2009). Modelling the effect of boundary scavenging on Thorium
1355 and Protactinium profiles in the ocean. *Biogeosciences*, 6, 3091-3107. doi: 10
1356 .5194/bg-6-3091-2009
- 1357 Sim, N. (2018). *Biogeochemical cycling of dissolved and particulate manganese*
1358 *in the northeast Pacific and Canadian western Arctic* (Doctoral dissertation,
1359 University of British Columbia). doi: 10.14288/1.0374222
- 1360 Smith, G. C., Roy, F., Mann, P., Dupont, F., Brasnett, B., Lemieux, J.-F., ...
1361 Bélair, S. (2014). A new atmospheric dataset for forcing ice-ocean models:
1362 Evaluation of reforecasts using the Canadian global deterministic prediction
1363 system. *Quarterly Journal of the Royal Meteorological Society*, 140(680),
1364 881-894. doi: 10.1002/qj.2194

- 1365 Spreen, G., Kwok, R., & Menemenlis, D. (2011). Trends in Arctic sea ice drift and
1366 role of wind forcing: 1992-2009. *Geophysical Research Letters*, *38*(19). doi: 10
1367 .1029/2011GL048970
- 1368 Stierle, A. P., & Eicken, H. (2002). Sediment inclusions in Alaskan coastal
1369 sea ice: Spatial distribution, interannual variability, and entrainment re-
1370 quirements. *Arctic, Antarctic, and Alpine Research*, *34*(4), 465-476. doi:
1371 10.1080/15230430.2002.12003518
- 1372 Stroeve, J. C., & Notz, D. (2018). Changing state of Arctic sea ice across all sea-
1373 sons. *Environmental Research Letters*, *13*(10). doi: 10.1088/1748-9326/
1374 aade56
- 1375 Stroeve, J. C., Serreze, M. C., Holland, M. M., Kay, J. E., Malanik, J., & Barrett,
1376 A. P. (2012). The Arctic's rapidly shrinking sea ice cover: A research synthe-
1377 sis. *Climatic Change*, *110*(3-4), 1005-1027. doi: 10.1007/s10584-011-0101-1
- 1378 Sunda, W. G., & Huntsman, S. A. (1994). Photoreduction of manganese oxides in
1379 seawater. *Marine Chemistry*, *46*(1-2), 133-152. doi: 10.1016/0304-4203(94)
1380 90051-5
- 1381 Tagliabue, A., Bowie, A. R., Boyd, P. W., Buck, K. N., Johnson, K. S., & Saito,
1382 M. A. (2017). The integral role of iron in ocean biogeochemistry. *Nature*,
1383 *543*(7643), 51-59. doi: 10.1038/nature21058
- 1384 The Pandas development team. (2020). Pandas-dev/pandas: Pandas. *Zenodo*, *21*, 1-
1385 9.
- 1386 Thyng, K. M., Greene, C. A., Hetland, R. D., Zimmerle, H. M., & DiMarco, S. F.
1387 (2016). True colors of oceanography: Guidelines for effective and accurate
1388 colormap selection. *Oceanography*, *29*(3), 9-13.
- 1389 Tilmes, S., Lamarque, J. F., Emmons, L. K., Kinnison, D. E., Marsh, D., Gar-
1390 cia, R. R., ... Blake, N. (2016). Representation of the Community Earth
1391 System Model (CESM1) CAM4-chem within the Chemistry-Climate Model
1392 Initiative (CCMI). *Geoscientific Model Development*, *9*(5), 1853-1890. doi:
1393 10.5194/gmd-9-1853-2016
- 1394 Tovar-Sánchez, A., Duarte, C. M., Alonso, J. C., Lacorte, S., Tauler, R., & Galbán-
1395 Malagón, C. (2010). Impacts of metals and nutrients released from melting
1396 multiyear Arctic sea ice. *Journal of Geophysical Research*, *115*(C7), C07003.
1397 doi: 10.1029/2009JC005685

- 1398 Tucker, W. B., Gow, A. J., Meese, D. A., Bosworth, H. W., & Reimnitz, E. (1999).
 1399 Physical characteristics of summer sea ice across the Arctic Ocean. *Journal of*
 1400 *Geophysical Research: Oceans*, *104*(C1), 1489-1504. doi: 10.1029/98jc02607
- 1401 Van Hulten, M., Middag, R., Dutay, J.-C., De Baar, H., Roy-Barman, M., Gehlen,
 1402 M., ... Sterl, A. (2017). Manganese in the west Atlantic Ocean in the context
 1403 of the first global ocean circulation model of manganese. *Biogeosciences*, *14*,
 1404 1123-1152. doi: 10.5194/bg-14-1123-2017
- 1405 Vieira, L. H., Achterberg, E. P., Scholten, J., Beck, A. J., Liebetrau, V., Mills,
 1406 M. M., & Arrigo, K. R. (2019). Benthic fluxes of trace metals in the Chukchi
 1407 Sea and their transport into the Arctic Ocean. *Marine Chemistry*, *208*, 43-55.
 1408 doi: 10.1016/j.marchem.2018.11.001
- 1409 Virtanen, P., Gommers, R., Oliphant, T. E., Haberland, M., Reddy, T., Cour-
 1410 napeau, D., ... others (2020). SciPy 1.0: fundamental algorithms for
 1411 scientific computing in Python. *Nature methods*, *17*(3), 261-272. doi:
 1412 10.1038/s41592-019-0686-2
- 1413 Waga, H., Eicken, H., Light, B., & Fukamachi, Y. (2022). A neural network-based
 1414 method for satellite-based mapping of sediment-laden sea ice in the Arctic. *Re-*
 1415 *remote Sensing of Environment*, *270*, 112861. doi: 10.1016/j.rse.2021.112861
- 1416 Wang, Q., Myers, P. G., Hu, X., & Bush, A. B. G. (2012). Flow constraints on
 1417 pathways through the Canadian Arctic Archipelago. *Atmosphere-Ocean*, *50*(3),
 1418 373-385. doi: 10.1080/07055900.2012.704348
- 1419 Wang, S., Bailey, D., Lindsay, K., Moore, J. K., & Holland, M. (2014). Impact of sea
 1420 ice on the marine iron cycle and phytoplankton productivity. *Biogeosciences*,
 1421 *11*(17), 4713-4731. doi: 10.5194/bg-11-4713-2014
- 1422 Waskom, M., & the Seaborn development team. (2020). *Seaborn*. Zenodo. doi: 10
 1423 .5281/zenodo.592845
- 1424 Wedepohl, H. K. (1995). The composition of the continental crust. *Geochimica et*
 1425 *Cosmochimica Acta*, *59*(7), 1217-1232. doi: 10.1016/0016-7037(95)00038-2
- 1426 Yamamoto-Kawai, M., Carmack, E. C., & McLaughlin, F. (2006). Nitrogen balance
 1427 and Arctic throughflow. *Nature*, *443*(7107), 43-43. doi: 10.1038/443043a
- 1428 Yamamoto-Kawai, M., McLaughlin, F. A., Carmack, E. C., Nishino, S., Shimada,
 1429 K., & Kurita, N. (2009). Surface freshening of the Canada Basin, 2003–2007:
 1430 River runoff versus sea ice meltwater. *Journal of Geophysical Research*,

1431 114(C1), C00A05. doi: 10.1029/2008JC005000

1432 Yeats, P. A., & Westerlund, S. (1991). Trace metal distributions at an Arctic Ocean
1433 ice island. *Marine Chemistry*, 33(3), 261-277. doi: 10.1016/0304-4203(91)
1434 90071-4

1435 Zalesak, S. T. (1979). Fully multidimensional flux-corrected transport algorithms for
1436 fluids. *Journal of Computational Physics*, 31(3), 335-362. doi: 10.1016/0021
1437 -9991(79)90051-2